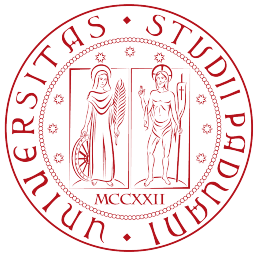

UNIVERSITÀ DEGLI STUDI DI PADOVA

Dipartimento di Fisica e Astronomia "Galileo Galilei"

Corso di Laurea Magistrale in Fisica

Tesi di Laurea

Thermal Evolution of Neutron Stars

Relatore

Prof. Roberto Turolla

Laureando

Davide De Grandis

Correlatore

Dr. Roberto Taverna

Anno Accademico 2017/2018

[…]we must conclude that all stars heavier than $1.5 M_\odot$ certainly possess regions in which the laws of quantum mechanics (and therefore of quantum statistics) are violated.

L. D. Landau (1932)

Contents

Abstract

Neutron stars (NSs) are astrophysical objects produced by the collapse of a stellar core in a supernova explosion when the degenerate pressure of neutrons halts the contraction. Under such conditions, to a first approximation matter is made of a plasma of nucleons ad electrons.

Such a system is governed by strong nuclear interactions, the collective properties of which are poorly known as yet. This leaves still open the question of what is the equation of state of mater at ultra-high densities. Many possible forms for this equation have been proposed, some of them predicting the presence of *exotic states* of matter, i.e., the formation of mesons, strange particles or even deconfined quarks at very high densities (several times the nuclear saturation density). The main tool to get information about the internal structure of a NS is the study of the reactions occurring in its interior. These produce neutrinos and photons, that subtract energy causing to the cooling of the star, that is born very hot after the collapse ($T \approx 10^{11}$K). Observations can provide the star age and surface temperature, allowing one to reconstruct its thermal history and hence inferring information about the physical processes at work in the interior.

In this work, the main processes involved in the thermal evolution of an isolated NS are considered, focusing on the different neutrino emission channels and on the effects of the presence of a superfluid phase in the core. Different reactions produce different thermal evolutions; in particular two main cooling scenarios can be identified, *fast cooling* and *slow cooling*. Albeit observations do not provide conclusive evidences, the comparison of models with data is not consistent with fast cooling at present. This put constraints on the equation of state, disfavouring those which predict the presence of exotic phases in the inner core.

Sommario

Le stelle di neutroni (NS) sono oggetti astrofisici prodotti quando il collasso di un nucleo stellare in un'esplosione di supernova viene arrestato dalla pressione di gas degenere dei neutroni. In tali condizioni, la materia è in prima approssimazione costituita da un plasma di nucleoni ed elettroni.

Le proprietà di questo sistema sono dunque dettate dalle caratteristiche dell'interazione forte, che non sono note nel dettaglio; in particolare, l'equazione di stato della materia ultradensa non è nota. Varie possibili forme di questa equazione sono state proposte, alcune delle quali prevedono la comparsa di cosiddetti stati esotici della materia, ossia la formazione di mesoni, particelle strane o deconfinamento di quark, a densità molto alte (diverse volte quella di saturazione nucleare). Lo strumento principale per accedere ad informazioni riguardanti la struttura di una NS è lo studio delle reazioni che avvengono al suo interno. Queste portano alla produzione di neutrini e fotoni, i quali sottraggono energia causando il raffreddamento della stella, che nelle fasi immediatamente successive al collasso è estremamente calda ($T \approx 10^{11}$K). Dalle osservazioni è possibile ricavare l'età e la temperatura superficiale della stella, in modo da seguirne l'evoluzione termica e quindi ricavare informazioni sui processi fisici in atto all'interno dell'oggetto.

Questo lavoro prende in considerazione i principali processi coinvolti nell'evoluzione termica di una NS isolata, con particolare attenzione ai diversi modi di emissione di neutrini e agli effetti della comparsa di fasi superfluide nel nucleo della stella. I diversi tipi di reazione producono differenti storie termiche; in particolare, possono essere individuati due scenari principali di raffreddamento, detti *fast cooling* e *slow cooling*. Sebbene le evidenze osservative non siano conclusive, il confronto dei modelli con i dati non mostra evidenze di processi che danno fast cooling. Questo pone dei vincoli alla forma delle possibili equazioni di stato, sfavorendo quelle che prevedono la formazione di stati esotici nelle zone più interne della stella.

Introduction

Neutron stars (NSs) are one of the possible final states of stellar evolution. The existence of astrophysical objects supported by the neutron degenerate gas pressure—in analogy to the case of white dwarfs, which are supported by electron degenerate gas pressure—was first proposed by F. Zwicky [Zwi33] and L. D. Landau [Lan37] in the 1930s and confirmed later on with the discovery of Pulsars (*Puls*ating st*ars*) in the 1960s. In particular, the first object to be identified as a NS was the pulsar at the center of the Crab Nebula in 1968 [Sca69].

As more observational data became available, different classes of NSs were identified. Most of the NSs discovered so far are radio pulsars, which are easily detectable from their pulsed emission. NSs can also be discovered from γ–ray or X–ray flares and other bursting events, that unveil their position. Among them, the most interesting objects are Magnetars (*Magnet*ic st*ars*), showing the strongest magnetic fields observed in the universe. Other important classes are given by NSs found at the center of a Supernova remnant, called Central Compact Objects (CCOs), and seven stars that were given the self–explaining name of X–ray dim isolates NSs (XDINSs).

NSs are the most compact objects in the universe without an event horizon, as they have masses of order of one solar mass ($M_\odot \simeq 1.99 \times 10^{33}\,\mathrm{g}$) and radii of order 10 km. This implies that the typical densities found in a NS are comparable to nuclear saturation density $\rho_0 = 2.8 \times 10^{14}\,\mathrm{g\,cm^{-3}}$, allowing one to test physics in regimes which are not accessible on Earth.

The interior of a NS is one of the most interesting yet mysterious environments in physics, where General Relativity, Nuclear and Particle Physics meet. This work will consider one of the main ways to study it: following the thermal evolution of the star. In fact, energy dissipation is due to processes depending on the composition of the object. Therefore, a model of the thermal history of NSs can be compared to observational data to obtain information of the internal composition. The work is organized as follows:

- in chapter 1 the general properties of NS are reviewed, including the GR structure equations;

- in chapter 2 the main cooling processes occourring in a NS are described;
- in chapter 3 the GR structure equations are solved and density and chemical composition profiles are calculated;
- in chapter 4 the cooling of NSs is described without taking into account the presence of superfluity in the core;
- in chapter 5 the effects of superfluidity are added, and predictions are compared with data.

1 | Neutron Stars

In this chapter the main general properties of NSs are reviewed. In particular, the internal structure and composition are considered, both from the point of view of the microscopic particle content and of the hydrostatic structure, that must be described in a general–relativistic framework.

1.1 Evolution

NSs are produced as the remnant of a Core–Collapse Supernova originating from a massive star, $10M_\odot \lesssim M \lesssim 25M_\odot$. In order to estimate the characteristics of the final object, one can assume that the angular momentum and the magnetic flux are conserved in the core collapse, i.e., that the SN explosion is spherically symmetric (or, at least, that the material is expelled radially) and that it does not produce a net charge flow. The latter assumption is much more realistic than the first one. Then, from conservation laws one can estimate the rotation period P to pass from the typical values of some days for ordinary stars to $P \sim 10^{-3}-10\,\mathrm{s}$: NSs are fast rotators. This fact is proven by the observation of radio–Pulsars, which exhibit periods exactly in the same range. Applying magnetic flux conservation yields typical values for magnetic fields of order $B \sim 10^{11}-10^{14}\,\mathrm{G}$, much higher than any other found in the universe. Note that to sustain such high magnetic fields currents are necessary, and hence a non negligible amount of charged particles must be present in the NS alongside neutrons (see section 1.3).

From an observational point of view, the most accessible data of a NS are the period, via time–domain observations, the luminosity and the temperature, via spectral analysis. Two quantities which have a very important role in the physics of NSs are the period P and its time derivative $\dot{P}$. NSs themselves are usually represented in the $P-\dot{P}$ diagram, fig. 1.1, which plays a similar role to that of the HR diagram for normal stars. In particular, different NS populations can be defined, the majority of stars being Radio Pulsars. Conversely, the mass of a NS is very difficult to measure unless it is in a binary system, and very few information about the radius can be obtained. To compare evolutionary models

with data, one of the key informations is the age of a NS. It can be estimated in several ways; the main ones are:

- the dynamic age, obtained studying the trajectory of the object with respect to its nearby stars. This is done by measuring the component of the velocity in the plane of the sky with optical observations and the perpendicular component with precise distance measurements. Then a trajectory is extrapolated backwards until a star cluster in which the NS may have formed is reached;

- the magneto–rotational age. Since NSs are spinning magnetized objects, they irradiate according to Larmor equation,

$$\dot{E} = \frac{2}{3c^3}|\ddot{\vec{\mathfrak{m}}}|^2 = \frac{B_{\mathrm{pol}}^2 R_{\mathrm{NS}}^6 \Omega^4}{6c^3} \sin^2 \xi, \tag{1.1}$$

  where B_{pol} is the intensity of the magnetic field at the magnetic pole and $\vec{\mathfrak{m}}$ is the magnetic dipole moment, forming an angle ξ with the rotation axis. This expression can be equated with the rotational energy loss (*spin-down luminosity*) $\dot{E}_{\mathrm{sd}} = I\Omega\dot{\Omega}$, where I is the moment of inertia. Finally, integrating the obtained equation (assuming the final angular velocity to be much smaller than the initial one) one can find an estimator for the NS age called *magneto–rotational characteristic age*,

$$\tau = \frac{1}{2}\frac{P}{\dot{P}}. \tag{1.2}$$

  This quantity has the advantage of depending only on P and $\dot{P}$, two relatively easy to measure parameters;

- the cooling age, obtained from the measurement of the temperature. In fact, many NSs show a thermal component in the emission spectrum, so that their temperature can be obtained from spectral observations. By comparing it with theoretically calculated *cooling curves*, i.e., the predicted age-temperature relation, a value for the age is obtained. The goal of this work is indeed to study this thermal evolution.

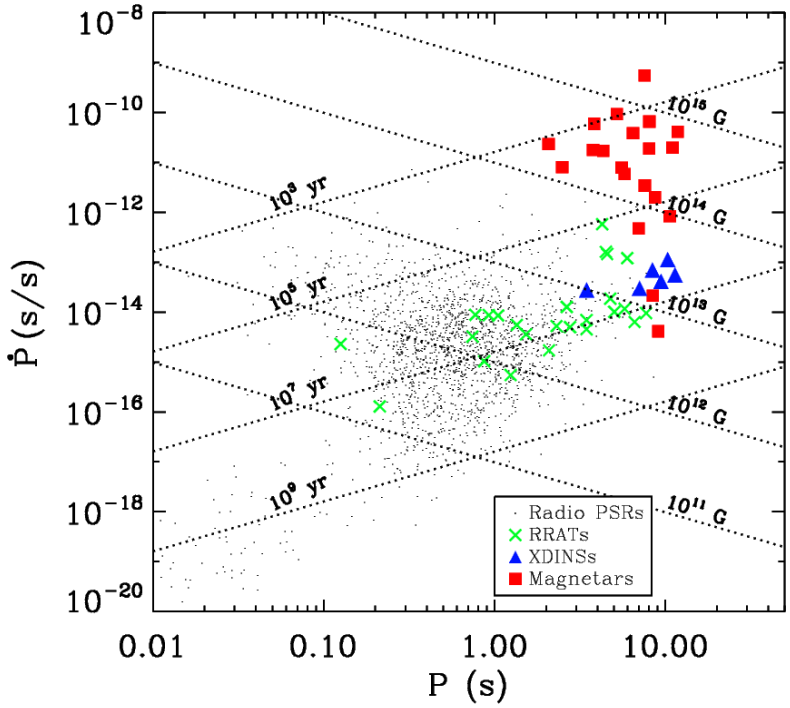

Figure 1.1: $P-\dot{P}$ diagram (double log–scale). Dashed lines with negative slope are the loci of constant B, positive slope ones the loci of constant τ. Different dingbats label different NS populations: black dots, that are the bulk of the total, label *radio–Pulsars*; crosses *Rotating radio transients*, stars similar to ordinary pulsars but showing irregual activity; triangles the so–called *X–ray dim isolated NSs* and squares *magnetars*, objects powered by their extremely strong magnetic field.

1.2 Internal structure

In a NS, matter undergoes extreme pressure and temperature conditions, causing the appearance of states of matter that are very different from laboratory situations. Loosely speaking, the inner regions of a NS resemble a gigantic atomic nucleus, while the outer parts are composed of ordinary atomic matter. The structure of the whole NS can be divided in several qualitatively different regions, as illustrated in fig. 1.2 (see [HPY07]):

- the *atmosphere*, composed of heavy elements (Fe, Ni) in gaseous state coming from the progenitor star, and H and He accreted from the interstellar medium. Since the surface gravity of a NS is huge, $g \approx 10^{14}\,\mathrm{cm\,s^{-2}} \approx 10^{11} g_{\oplus}$, it is geometrically very thin (few cm) but it can be optically thick;
- the *ocean*, consisting in a Coulomb liquid of electrons and nuclei. The high surface gravity produces a stratification of the different chemical species with different densities;
- the *crust*, $\sim$ 1km thick, contains electrons and nuclei. As the density increases, nuclei become more and more neutron rich (since β capture is favoured by the degeneracy of electrons) until free neutrons appear at the *neutron drip density* $\rho_d = 4.3 \times 10^{11}\,\mathrm{g\,cm^{-3}}$;
- the *mantle* is a region in which nuclei are embedded in a sea of quasi free neutrons. Under these conditions, nuclei get deformed assuming rod–like and plate–like shapes, forming a phase called *nuclear pasta* [RPW83]. The thermodynamical stability of nuclear pasta, and hence the very existence of the mantle, depends on the details of nuclear interaction and is still an open issue;
- the *outer core*, a region of density $0.5\rho_0 \lesssim \rho \lesssim 2\rho_0$. It is usually few kilometers thick and contains most of the matter of the star. At these densities nuclei cannot be bound, and matter consists of a plasma of nucleons and leptons (called $npe\mu$ *matter*);
- the *inner core*, which is present only in stars with $M \gtrsim 1.5 M_{\odot}$, in which densities are several times ρ_0. The details of its composition are still unknown, but it is probably more complicated than that of the outer core. The most studied hypotheses are:
  - hyperonization of matter, i.e., the appearance of heavy particles, mainly Λ^- and Σ^+ hyperons, giving the so–called $npe\mu\Lambda\Sigma$ *matter*;
  - the formation of a Bose–Einstein condensate of π mesons;

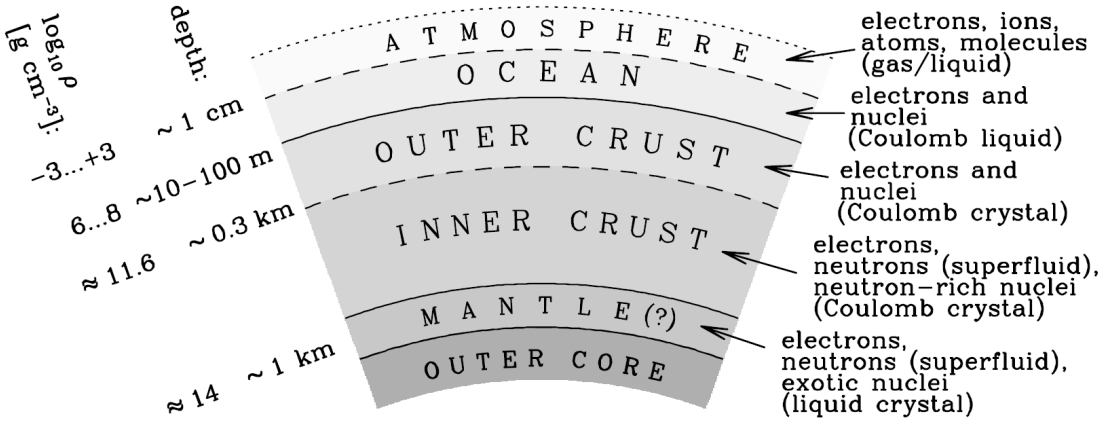

Figure 1.2: Schematic representation of a NS interior, from [HPY07]

- the formation of a similar BE condensate of K mesons;
- the formation of a quark–gluon plasma.

The last three scenarios are called *exotic* states. The composition of the NS inner core is one of the main open issues in modern astrophysics.

1.3 β equilibrium

Since the outer core contains the vast majority of the whole mass, a NS can be studied to a first approximation as a plasma of neutrons, protons and electrons (npe matter) at β equilibrium. The pressure supporting the object is provided by the degeneracy of neutrons, which is a characteristic feature of fermionic particles. In NS matter also electrons are completely degenerate. This fact is important since the phase space accessible to electrons produced in weak reactions is reduced, putting constraints to the reactions themselves.

A system of fermions at thermodynamic equilibrium is described by the Fermi–Dirac distribution

$$f(T) = (e^{(E-\mu)/T} + 1)^{-1} \tag{1.3}$$

where μ is the chemical potential. In the limit $T \to 0$, this distribution reduces to a step function $\Theta(E_F - E)$, where the *Fermi energy* E_F is the value $\mu(T = 0)$. In this situation, all the energy states are occupied up to the Fermi energy, while the others are empty. This is the case of *complete degeneracy*. In a NS one can make

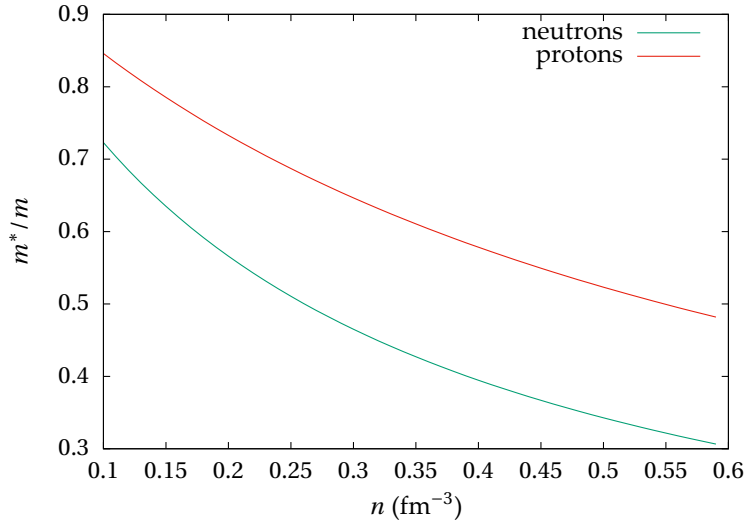

Figure 1.3: Landau effective mass under NS conditions for Sk4 EoS (see section 1.5).

the assumption of complete degeneracy, since the Fermi temperature $T_F = k_B E_F$ is always much higher than the star temperature. Therefore, the whole star is thought to be at absolute zero but for the states that are very close to Fermi energy. In momentum space, the momentum for which $E_F = \sqrt{p^2 + m^2}$ is called *Fermi momentum* p_F, and the corresponding state are said to lie on the *Fermi sphere* surface. At first order near the Fermi sphere, we can approximate

$$E - E_F \simeq v_F(p - p_F), \tag{1.4}$$

where the "velocity" of particles on the Fermi surface is

$$v_F^i = \left.\frac{\partial E}{\partial p_i}\right|_{p=p_F}. \tag{1.5}$$

Then, in analogy to classical physics one introduces the *(Landau) effective mass* $m^* = p_F / v_F$, that will of course depend on the interactions that particles undergo. In fig. 1.3 the effective mass for the Skyrme nuclear potential in NS core conditions (see 1.5) is displayed. One can prove that $m^* > 0$ [LLP77].

Under complete degeneracy assumption, Fermi momentum can be expressed as a function of the particle number density n,

$$p_F = \left(\frac{3}{8\pi}\right)^{1/3} \frac{h}{mc} n^{1/3} \qquad x_F = \frac{\hbar p_f}{mc}, \tag{1.6}$$

where we introduced the *reduced Fermi momentum* x_F.

In a NS, the Fermi energy is enough to compensate the proton-neutron mass defect $D \equiv m_n - m_p \simeq 1.3\,\mathrm{MeV}$, so that the process of *inverse β decay* (or *neutronization*) is allowed,

$$p\ e^- \rightarrow n\ \nu_e.$$

Eventually, this process reaches chemical equilibrium with ordinary β decay,

$$n \rightarrow p\ e^-\ \bar{\nu}_e$$

whose efficiency is limited by the fact that in complete degeneracy conditions there is only a small phase space left for the outcoming electron. The equilibrium situation is expressed by the Saha equation,

$$\mu_e + \mu_p = \mu_n \tag{1.7}$$

where the neutrino chemical potential has been neglected, $\mu_\nu = 0 = \mu_{\bar{\nu}}$ (see section 2.4).

At zero temperature, chemical potentials are given by Fermi energies so that eq.1.7 reads

$$m_e c^2 \sqrt{1 + x_e^2} + m_p c^2 \sqrt{1 + x_p^2} = m_n c^2 \sqrt{1 + x_n^2} \tag{1.8}$$

where $x_a = x_F$ for particle a. This equation can be combined with charge neutrality condition,

$$n_e = n_p \implies (x_e m_e)^3 = (x_p m_p)^3 \tag{1.9}$$

to obtain the neutron to proton ratio R in the NS,

$$R = \frac{n_n}{n_p} \simeq \frac{x_n^3}{x_p^3} = \frac{x_n^3}{\left[\frac{x_n^4 + 4D x_n^2/m_n + 4(D^2 - m_e^2)/m_n^2}{4(1+x_n^2)}\right]^{3/2}} \tag{1.10}$$

which can be related to mass density as

$$\rho = m_n n_n \left(1 + \frac{n_p}{n_n}\right) = m_n \frac{8\pi}{3} \left(\frac{m_n c}{h}\right)^3 x_n^3 \left(1 + \frac{1}{R}\right). \tag{1.11}$$

Taking this relation to the high density limit, one sees that the ratios between the number densities of the particles go as $n_n : n_p : n_e = 8 : 1 : 1$, see fig. 1.4. This relation can be used as a rule–of–thumb for the whole NS; in particular, the presence of charged particles is crucial for the generation of magnetic fields.

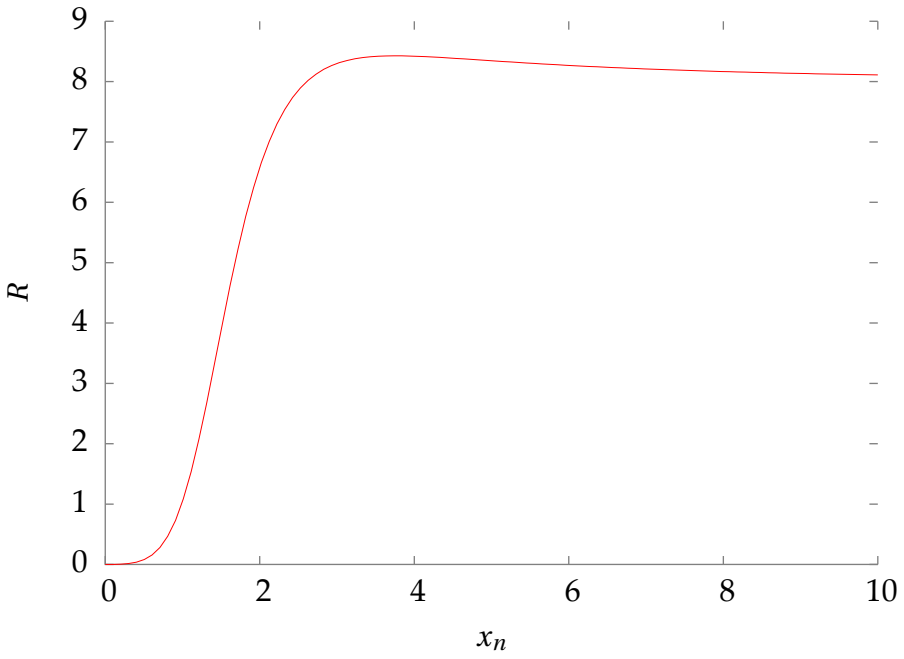

Figure 1.4: The neutron to proton ratio R as a function of $x_n \propto n^{1/3}$.

1.4 Hydrostatic equilibrium

An isolated NS can be treated to an excellent extent as a spherically symmetric system. The spacetime around the object, $r > R$, is described by the spherically symmetric solution of Einstein's equations *in vacuo*, the well known Schwarzschild metric [Sch16] that, expressed in spherical coordinates (r, θ, φ) adapted to a stationary observer, reads

$$\mathrm{d}s^2 = -\left(1 - \frac{R_S}{r}\right)\mathrm{d}t^2 + \left(1 - \frac{R_S}{r}\right)^{-1}\mathrm{d}r^2 + r^2\mathrm{d}\Omega^2 \tag{1.12}$$

where $\mathrm{d}\Omega^2 = \mathrm{d}\theta^2 + r^2\sin^2\theta\,\mathrm{d}\varphi^2$ and we introduced the *Schwarzschild radius*

$$R_S = \frac{2GM}{c^2} = 2R_g \tag{1.13}$$

where M is the mass of the star; the quantity R_g is called the *gravitational radius*. A NS has a physical radius of few R_S. For comparison, for the Sun it is $R/R_S \approx 2 \times 10^5$. Strictly speaking, the assumption of spherical symmetry breaks down if the star is rotating. However, an analytic solution for Einstein's equations in cylindrical symmetry is known only in vacuo [Ker63] and it does not allow a smooth connection with an "internal" solution, describing a region filled with

matter: therefore, it cannot be used to describe the surroundings of a rotating NS. Moreover, the typical rotation speed of a NS is such that the differences with respect to the static solution are negligible (the adimensional angular momentum is $a = I\Omega/Mc \approx 10^{-21}$). Also the presence of a magnetic field breaks the symmetry. In a NS it can acquire very high values, up to 10^{14} G and, to a first approximation, it has the form of a dipole. This introduces a non negligible component of the stress–energy tensor $T^{\mu\nu}$ that does not respect spherical symmetry. In any case, in this work only weakly magnetized stars will be considered.

The presence of matter at $r < R$ modifies the metric. Assuming matter to be described by the stress-energy tensor of a perfect fluid with energy density ρ, pressure p and 4–velocity u^μ,

$$T^{\mu\nu} = (p/c^2 + \rho)\, u^\mu u^\nu + p g^{\mu\nu} \overset{\text{rest frame}}{=} \text{diag}(\rho c^2, p, p, p) \tag{1.14}$$

the metric becomes

$$\mathrm{d}s^2 = -\mathscr{R}^2 c^2 \mathrm{d}t^2 + \mathscr{V}^2 \mathrm{d}r^2 + r^2 d\Omega^2 \tag{1.15}$$

having defined the quantities [Tho77]

$$\mathscr{R} = (\text{redshift correction factor}) = \exp\left(\Phi/c^2\right) \tag{1.16}$$

$$\mathscr{V} = (\text{volume correction factor}) = \left(1 - \frac{2GM_T(r)}{rc^2}\right)^{-1/2} \tag{1.17}$$

$$\mathscr{G} = (\text{gravitational acceleration correction factor}) = \frac{M_T(r) + 4\pi r^3 p/c^2}{M(r)} \tag{1.18}$$

where $M(r)$ is the rest mass inside a sphere of radius r, $M_T(r)$ is the total mass (including the gravitational binding energy) in the same sphere and the gravitational potential Φ is given by

$$\frac{\mathrm{d}\Phi}{\mathrm{d}r} = -\frac{\mathrm{d}p}{\mathrm{d}r}\left(\frac{1}{p(r) + \rho(r)c^2}\right) \tag{1.19}$$

with the boundary condition $\Phi(R) = 1 - R_S/R$. This ensures that for $r = R$ the internal metric connects smoothly with 1.12.

In this setup, hydrostatic equilibrium is described by the Tolman–Oppenheimer–Volkoff (TOV) equation [OV39],

$$\frac{\mathrm{d}p}{\mathrm{d}r} = -\frac{GM(r)\rho}{r^2}\left(1 + \frac{\Pi - B}{c^2} + \frac{p(r)}{\rho c^2}\right)\mathscr{G}\mathscr{V}^2 \tag{1.20}$$

where Π and B are the specific internal energy and the binding energy per unit mass respectively, and the density $\rho(r)$ satisfies the equation

$$\frac{\mathrm{d}M}{\mathrm{d}r} = 4\pi r^2 \rho(r). \tag{1.21}$$

Since we are considering degenerate matter at $T = 0$, $\Pi - B = 0$.

The total radius of the star is determined by the condition $p(R) = 0$.

In order to study nuclear matter, it is convenient to introduce the *baryon number density* $n_b(r)$. Then, the total baryon number of the star is

$$A_b = 4\pi \int_0^R n_b(r) \mathcal{V} r^2 dr. \tag{1.22}$$

and the baryon number in a sphere of radius r, $a_b(r)$, is given by the equation [HPY07]

$$\frac{\mathrm{d}a_b}{\mathrm{d}r} = 4\pi r^2 n_b \left(1 - \frac{2GM(r)}{rc^2}\right)^{-1/2} \tag{1.23}$$

with boundary conditions $a_b(0) = 0$ and $a_b(R) = A_b$. The mass density is given by $\rho_b(r) = m_b a_b$ where m_b is the mass of the considered baryon. Conventionally, data found in in literature are expressed in unit atomic mass $m_u = 931.09\,\mathrm{MeV}$.

A consistent model of NS structure is built integrating the coupled equations 1.19, 1.20, 1.21, 1.23 and an equation of state (EoS) $p = p(\rho)$ (or $\rho = \rho(p)$) to give the pressure or density profile of the star. The first two equations and the EoS form a closed system by themselves.

1.5 The EoS

In most ordinary stellar models a *polytropic* equation of state $p = K\rho^\gamma$ is used. However, the peculiar conditions of matter in NSs require the use of more sophisticated equations, calculated considering the properties of nuclear matter, including the (still poorly known) form of nuclear strong potential. The equation of state of ultradense matter to be used to solve the structure of the object is an open problem, complicated by the fact that it involves nuclear physics, condensed matter physics and particle physics altogether, considered in regimes which are not their customary ones. The outer core is the easier region to treat, since it can be considered to a good extent a npe plasma described in §1.3. The same ideas can be used to extend this model to the presence of free muons ($npe\mu$ matter). Conversely, the inner core requires a model accounting for hyperonization and other exotic states. The EoS of the crust is a problem of the opposite kind: whereas the fundamental physics involved is quite well known, the system poses problems of atomic and solid–state physics that are very difficult to treat consistently, in regimes where ground based expriments cannot be conclusive.

The main techniques to obtain these equations are numerical calculation based on Hartree-Fock-Bogoliubov and Mean–field methods. In this work different types of EoS are considered. In particular, two of them, labeled Sk4 and Sk6, are

obtained using mean field methods with an effective potential for nuclear force known as *Skyrme potential*. Its general parametrization in configuration space is

$$\begin{aligned}\hat{V}(\vec{r}_1,\vec{r}_2) = {} & t_0\,(1+x_0\hat{P}_\sigma)\delta(\vec{r}_1-\vec{r}_2) + \frac{t_3}{6}(1+x_3\hat{P}_\sigma)\,\delta\left(\frac{1}{2}(\vec{r}_1+\vec{r}_2)\right)\delta(\vec{r}_1-\vec{r}_2) \\ & -\frac{t_1}{2}\left(1+x_1\hat{P}_\sigma\right)\left((\nabla_1-\nabla_2)^2\delta(\vec{r}_1-\vec{r}_2)+\text{h.c.}\right) \\ & -t_3\left(1+x_2\hat{P}_\sigma\right)((\nabla_1-\nabla_2)\,\delta(\vec{r}_1-\vec{r}_2)(\nabla_1-\nabla_2)) \\ & -i\,t_4(\nabla_1-\nabla_2)\,\delta(\vec{r}_1-\vec{r}_2)\,(\nabla_1-\nabla_2)(\hat{\sigma}_1+\hat{\sigma}_2); \\ \hat{P}_\sigma = {} & \frac{1}{2}(1+\hat{\sigma}_1\cdot\hat{\sigma}_2)\end{aligned} \tag{1.24}$$

where $\hat{\sigma}$ is a Pauli matrix and $\hat{P}_\sigma$ is the so–called *spin exchange operator*. The scalar quantities $t_{0\ldots4}$ and $x_{0\ldots3}$ are phenomenological parameters obtained fitting nuclear physics data. Many different choices of their values are possible, corresponding to different EoSs: the EoSs used in this work are obtained using the procedure described in [GR15] with the parameters obtained from different data set in [RF95] (Sk4) and [ASA05] (Sk6). Another EoS that will be used is the one by Akmal, Pandharipande and Ravenhall (therefore labeled APR) [APR98] based on variational methods for matter at β equilibrium with corrections accounting for relativistic effects of order $(v/c)^2$ and three–nucleons interactions. This EoS is considered as a standard for many astrophysical applications. The last one (labeled Quark) is an equation obtained with relativistic mean field techniques taking into account the presence of free quarks in the inner core [She+98].

In general, an EoS is called *stiff* or *soft* depending on the amount of pressure change for a given increase in density. A stiff equation corresponds to a material that is harder to compress and thus offers more support against gravity. Conversely, a soft equation of state produces a smaller increase of pressure for a given change in density. In this case, the "Quark" EoS is the softest, the "Sk4" the stiffest.

The data for the EoSs used in this work are taken from the online database of the CompStar collaboration[CompOSE].

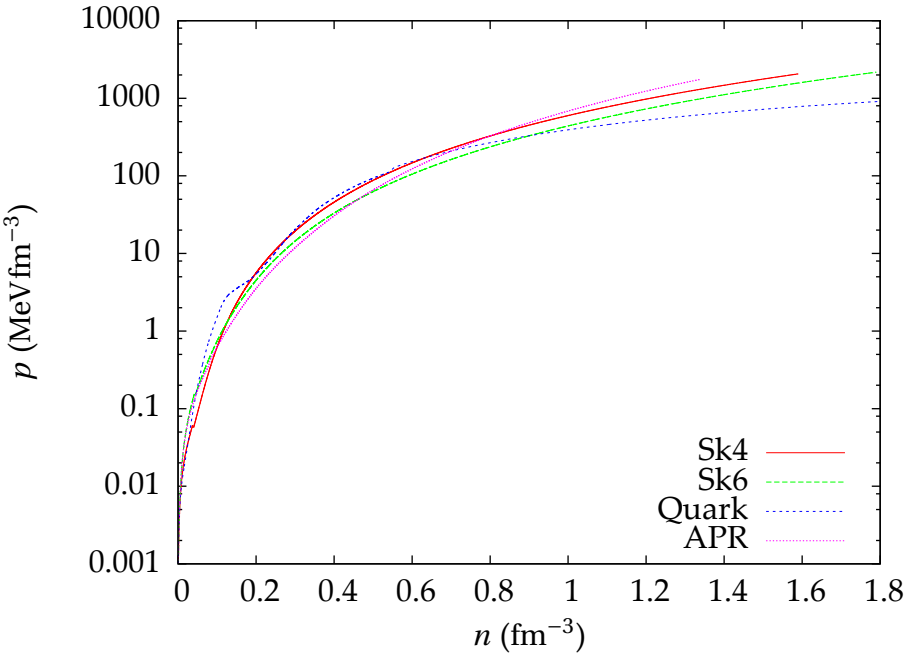

Figure 1.5: Examples of EoSs shown as functions of the number density.

2 | Cooling processes

A NS can cool down by the emission of gravitational radiation, electromagnetic radiation and neutrinos. For an isolated object, the mass quadrupole moment and rotational speed are so small that gravitational wave emission is negligible. Qualitatively, one can distinguish three cooling stages [Gus+04]. In the first ("non-isothermal") stage, $t \lesssim 100\,\mathrm{y}$, the main cooling mechanism is neutrino emission but the stellar interior stays highly non–isothermal and a significant fraction of the emission comes from the crust. In the second ("neutrino") stage, $10^2 \lesssim t \lesssim 10^5\,\mathrm{y}$, the cooling proceeds mainly via neutrino emission from the isothermal interior. In the third ("photon") stage, $t \gtrsim 10^5\,\mathrm{y}$, the star cools predominantly through surface photon emission.

The dissipation of magnetic fields can give rise to heating terms. In this work, lowly (for astrophysical standard, $B \lesssim 10^{12}\,\mathrm{G}$) magnetized NS are considered, so that this effect is negligible.

2.1 The Cooling equations

The thermal evolution of a NS can be described by the GR generalization of heat transport equation in the interior, [Vig13]

$$c_v \mathscr{R} \frac{\partial T}{\partial t} + \vec{\nabla} \cdot (\mathscr{R} \vec{\mathscr{F}}) + \mathscr{V} H = -\mathscr{R} Q \tag{2.1}$$

where $\mathscr{R}$ is defined in 1.16 and

- c_v is the heat capacity per unit volume;
- $\vec{\mathscr{F}}$ is the thermal flux, which in the diffusion limit is given by

$$\mathscr{F}_i = -\mathscr{V}^{-1/2} \kappa_{ij} \partial_j (\mathscr{V}^{1/2} T) \tag{2.2}$$

  where κ is the thermal conductivity tensor, $i, j = 1, 2, 3$ and Einstein index convention is used;

- H and Q are the heating rate and the energy loss rate per unit volume;
- the gradient is to be taken accordingly to the metric,

$$\vec{\nabla} = (\mathscr{V}^{-1}\partial/\partial r, r^{-1}\partial/\partial\theta, (r\sin\theta)^{-1}\partial/\partial\varphi).$$

The heating term H can be due to accretion or to magnetic energy dissipation: for an isolated and weakly magnetized NS, we can set $H = 0$. Moreover, anisotropies in the transport properties of matter are due to the magnetic field, so that neglecting it reduces the whole problem to a one–dimensional one. In this case, the gradient reduces to a simple derivative, and so the second order parabolic PDE 2.1 can be re–expressed as the set of two first order PDEs [Pag98],

$$\begin{cases} \dfrac{\partial(L\mathscr{R}^2)}{\partial r} \equiv \dfrac{\partial\mathscr{L}}{\partial r} = -4\pi r^2\mathscr{R}\mathscr{V}\left(c_v\dfrac{\partial T}{\partial t} + \mathscr{R}Q\right) \\ \dfrac{\partial(T\mathscr{R})}{\partial r} \equiv \dfrac{\partial\mathscr{T}}{\partial r} = \dfrac{1}{\kappa}\dfrac{L}{4\pi r^2}\mathscr{R}\mathscr{V}, \end{cases} \tag{2.3}$$

where the function L is the luminosity of the object. If the emission is purely thermal, like in the case of most main sequence stars, luminosity is given by the Stefan–Boltzmann law,

$$L_\gamma = 4\pi R^2\eta\sigma T^4 \tag{2.4}$$

where $\eta \sim 1$ is the emissivity. In this case, however, an important contribution—the main one, at some stages—comes from neutrino emission. Then, the total luminosity L comes from two contributions: L_γ and a "neutrino luminosity" L_ν, defined as the energy lost via neutrinos per unit time. This quantity per unit volume is the emissivity Q of eq. (2.1).

2.2 Effects of the envelope

Despite being geometrically thin, the effect of the envelope (the regions surrounding the core) is not negligible due to its non trivial optical and thermal properties. Therefore, the widespread approach is to split the star in two parts: bulk properties are computed with eq. (2.1) from the center to the bottom of the envelope, while the envelope itself is treated in plane–parallel approximation. This produces a relation between the temperature T_b at the bottom of the envelope and the surface temperature T_s, that is in general expressed by Tsuruta law [Tsu64], $T_s \sim T_b^{1/2+\alpha}$ with $\alpha \ll 1$. For a NS with an envelope composed mostly of iron, a more precise relation was obtained by [GPE83],

$$T_{8,b} = 1.288\left(\frac{T_{6,s}^4}{g_{14}}\right)^{0.455} \tag{2.5}$$

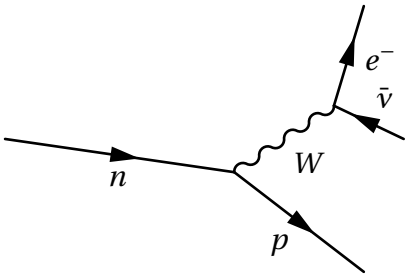

Figure 2.1: Tree level Feynman diagram for β decay.

where g_{14} is the NS surface gravity in units of $10^{14}\,\mathrm{cm\,s^{-2}}$ and T_k is the temperature in units of 10^kK. This law will be used in the simulations described in chapter 4 and chapter 5, since an iron envelope is the most realistic assumption for an isolated NS, which did not accrete much light elements from the surrounding medium.

2.3 Neutrino processes

As it has already been pointed out in section 2.1, a NS is a huge neutrino emitter. A great wealth of different neutrino reactions happen both in the crust and in the core. In this section the most important reactions for neutrino cooling of NSs are reviewed. In general, the *neutrino emissivity* Q of a process (having dimensions of energy per unit time per unit volume) can be defined as [YGH01][FM79]

$$Q_\nu = \int \prod_{i,j} \frac{\mathrm{d}^3 p_i}{(2\pi)^3 2E_i} \frac{\mathrm{d}^3 p_j}{(2\pi)^3 2E_j} (2\pi)^4 \delta^{(4)}\left(\sum_j p_j - \sum_i p_i\right) \varepsilon_\nu f_i (1 \pm f_j) |\overline{M}_{ji}|^2 \qquad (2.6)$$

where i, j label the initial and final state particles respectively, ε_ν is the energy emitted via neutrino loss per reaction, $\overline{M}_{ij}$ is the unpolarized Feynman amplitude of the process and $f_k = f_k(E_k, T, \mu_k)$ is the distribution function of particle k. The factors $(1 \pm f_j)$ are the so–called *Bose enhancement* for bosons (with "+" sign), or *Pauli suppression* for fermions (with "−" sign).

Urca process As it has already been mentioned in §1.3, the most obvious process in a NS is

$$\begin{cases} p\ e^- \to n\ \nu_e \\ n \to p\ e^-\ \bar{\nu}_e \end{cases} \qquad (2.7)$$

which is called the *Urca* (or *Direct Urca, dUrca*) process. This process is on threshold: it is kinematically allowed only if $p_n < p_p + p_e$, i.e., the particle momenta

direct Urca			$Q = (10^{23} - 10^{27})\, T_9^6\, \mathrm{erg\,cm^{-3}\,s^{-1}}$
$\begin{cases} p\ l \to n\ \nu_l \\ n \to p\ l\ \bar{\nu}_l \end{cases}$	$\begin{cases} p\ l \to \Lambda\ \nu_l \\ \Lambda \to p\ l\ \bar{\nu}_l \end{cases}$	$\begin{cases} n\ l \to \Sigma\ \nu_l \\ \Sigma \to n\ l\bar{\nu}_l \end{cases}$	$\begin{cases} \Lambda\ l \to \sigma\ \nu_l \\ \Sigma \to \Lambda\ l\ \bar{\nu}_l \end{cases}$
modified Urca			$Q = (10^{18} - 10^{21})\, T_9^8\, \mathrm{erg\,cm^{-3}\,s^{-1}}$
$\begin{cases} pp\ l \to pn\ \nu_l \\ pn \to pp\ l\ \bar{\nu}_l \end{cases}$	$\begin{cases} np\ l \to nn\ \nu_l \\ nn \to np\ l\ \bar{\nu}_l \end{cases}$	$\begin{cases} HNl \to NH\ \nu_l \\ HN \to HNl\bar{\nu}_l \end{cases}$	
bremsstrahlung			$Q = (10^{16} - 10^{20})\, T_9^8\, \mathrm{erg\,cm^{-3}\,s^{-1}}$
$nn \to nn\nu\bar{\nu}$	$np \to np\nu\bar{\nu}$	$pp \to \nu\bar{\nu}$	$B_1B_2 \to B_1B_2\nu\bar{\nu}$
superfluid processes			$Q = (10^{18} - 10^{21})\, T_9^7\, \mathrm{erg\,cm^{-3}\,s^{-1}}$
$B \to B\nu\bar{\nu}$			

Table 2.1: Main neutrino reaction in a NS core. Here, B stands for any baryon, l for any lepton, N for any nucleon and H for any hyperon. Some order–of–magnitude values for the emissivities are provided. Note that the general form is $Q = Q_0 T^k$.

must satisfy the triangle inequality. In complete degeneracy conditions the momenta to be used are Fermi momenta, and using eq. (1.6) this inequality can be translated into $n_e/n_n < 1/9$. This condition is not met in β equilibrium matter, where $n : p : e = 8 : 1 : 1$ and is almost never satisfied in realistic conditions. It is allowed only in the NS inner core by some stiff EoS (for densities several times ρ_0). However, if the threshold is met dUrca becomes the most efficient neutrino emission mechanism by several orders of magnitude compared to any other process described hereafter. Therefore, the triggering of dUrca processes is a key point for NS cooling.

The emissivity Q_ν^d (d stands for direct) can be obtained by doubling the emissivity of the β decay reaction obtained using $f = \Theta(p - p_F)$, and the Feynman amplitude from diagram 2.1*

$$Q_\nu^d = 4.00 \times 10^{27} \left(\frac{n_e}{n_0}\right)^{1/3} \frac{m_n^* m_p^*}{m_n^2}\, T_9^6\, \Theta_{npe}\, \mathrm{erg\,cm^{-3}\,s^{-1}} \tag{2.8}$$

where T_9 is the temperature in units of 10^9 K and $\Theta_{npe} = 1$ if the Fermi momenta p_F^e, p_F^n and p_F^p satisfy the triangle inequality, and is 0 otherwise.

*In the diagrams the charged and neutral currents of WGS electroweak theory [Wei64] are shown for clarity sake, but the results were calculated in the Fermi effective theory limit.

Process		r_{12}
$\Lambda \to p l \bar{\nu}_l$	$pl \to \Lambda \nu_l$	0.039
$\Sigma \to n l \bar{\nu}_l$	$nl \to \Sigma \nu_l$	0.012
$\Sigma \to \Lambda l \bar{\nu}_l$	$\Lambda l \to \Sigma \nu_l$	0.206

Table 2.2: Values of the effective coupling in eq. (2.10) for different hUrca processes.

μUrca and hUrca processes The presence of muons or hyperons can produce reactions which are analogous to the Urca process, where the μ replaces the electron or an hyperon replaces the nucleons,

$$\begin{cases} p\ \mu^- \to n\ \nu_\mu \\ n \to p\ \mu^-\ \bar{\nu}_\mu \end{cases} \qquad \begin{cases} H_2\ l^- \to H_1\ \nu_l \\ H_1 \to H_2\ l^-\ \bar{\nu}_l \end{cases} \tag{2.9}$$

where H_i stands for an hyperons and l for any lepton. In the first case the only difference is that the threshold condition involves the Fermi momentum of the muon, yielding a higher threshold density (still depending on the EoS) with the same emission rate. Conversely, the hyperon reaction differs also for the coupling constants, thus the emissivity is different. The hyperons expected to appear in a NS are $\Lambda^{\pm}$ and Σ^- (some very peculiar EoSs predict also $\Xi^{0,\pm}$ and Σ^0). The corresponding emissivity is analogous to the direct Urca one,

$$Q_\nu^{dh} = 4.00 \times 10^{27} \left(\frac{n_e}{n_0}\right)^{1/3} \frac{m_1^* m_2^*}{m_n^2}\, T_9^6\, \Theta_{12l}\, r_{12}\, \mathrm{erg\,cm^{-3}\,s^{-1}} \tag{2.10}$$

where 1 and 2 label the hyperons and the coefficient r_{12} accounts for the different coupling, and is given in table 2.2.

mUrca process In the regions where kinematic constraints block direct Urca reactions—which for the majority of EoSs corresponds to the whole star—cooling proceeds through higher–order processes. These reactions are the so–called *modified Urca* (mUrca) process, consisting in a Urca process mediated by a by–standing nucleon,

$$\begin{cases} p\ p \to p\ n\ e^+ \nu \\ n\ p \to p\ p\ e^-\ \bar{\nu} \end{cases} \qquad \begin{cases} n\ p \to n\ n\ e^+ \nu \\ n\ n \to n\ p\ e^-\ \bar{\nu}. \end{cases} \tag{2.11}$$

The momentum provided by the bystander allows to overcome the kinematic limitations. This process produces neutrinos of electron flavour only. The main

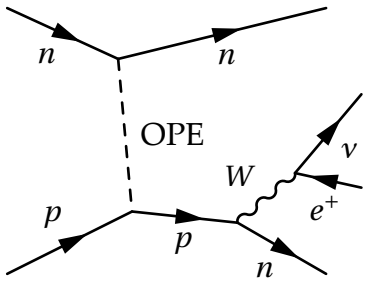

Figure 2.2: One of the tree–level Feynman diagrams for mUrca process (neutron branch). The dashed line indicates an effective nucleon–nucleon interaction.

problem in describing this process is that—differently from dUrca— the leading contribution does not come from weak interactions only, but it depends of the nucleon–nucleon strong interaction as outlined in the diagram 2.2. Following [FM79] and [YGH01], the results hereafter mentioned are calculated in the OPE (one pion exchange) long–range effective theory.

The two processes described in eq. (2.11) are called *proton branch* and *neutron branch* respectively. The emission rate of the neutron branch can be again calculated according to eq. (2.6), yielding

$$Q_\nu^{mn} \simeq 6.22 \times 10^{21} \alpha\beta \left(\frac{m_n^*}{m_n}\right)^3 \left(\frac{m_p^*}{m_p}\right) \left(\frac{n_p}{n_0}\right)^{1/3} T_9^8 \mathrm{erg\,cm^{-3}\,s^{-1}} \tag{2.12}$$

where $\alpha = 1.13$ and $\beta = 0.68$ are phenomenological parameters introduced in [FM79] to account for screening and correlation terms in a simplified framework. Then, the proton branch emissivity can be found through the relation

$$\frac{Q_\nu^{mn}}{Q_\nu^{mp}} = \left(\frac{m_p^*}{m_n^*}\right)^2 \frac{(p_F^e + 3p_F^p - p_F^n)^2}{8 p_F^e p_F^p} \Theta_{mp} \tag{2.13}$$

which is not dependent on the particular model of strong interaction. The main feature if this relation is the presence of a threshold $\Theta_{mp} = 1$ if $p_F^n < 3p_F^p + p_F^e$ or 0 otherwise. For β equilibrium npe matter, this condition is translated to densities in $n_p/n_{\mathrm{tot}} > 1/65 = 0.0154$. This condition is met almost everywhere for the majority of EoSs in a NS core. The proton branch is not as efficient as the neutron one, but its contribution is not negligible, especially at high density. For example, near the dUrca threshold density, $Q_\nu^{mp}/Q_\nu^{mn} \simeq 1/2$.

Bremsstrahlung Due to neutral weak currents, the mUrca process is not the only one to determine neutrino emission. In fact, a contribution comes also from

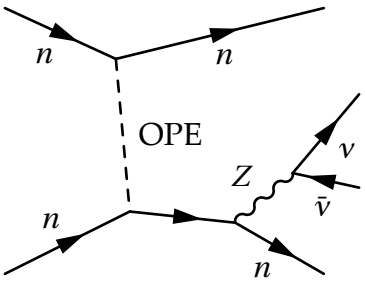

Figure 2.3: One of the tree level Feynman diagrams for bremsstrahlung process. The dashed line indicates an effective nucleon–nucleon interaction.

neutrino bremsstrahlung in particle–particle scattering. The related processes are

$$nn \to nn\nu\bar{\nu} \qquad pp \to pp\nu\bar{\nu} \qquad np \to np\nu\bar{\nu} \tag{2.14}$$

which at tree–level are described by diagram 2.3 and the analogous ones. These are similar to the mUrca processes, but involving neutral currents; therefore, they produce neutrinos of all flavours. The correspondent emissivities are [YGH01]

$$\begin{aligned} Q_\nu^{nn} =& 2.48\times10^{19}\left(\frac{m_n^*}{m_n}\right)^4\left(\frac{n_n}{n_0}\right)^{1/3}\mathcal{N}_\nu\, T_9^8\,\mathrm{erg\,cm^{-3}\,s^{-1}} \\ Q_\nu^{pp} =& 5.78\times10^{18}\left(\frac{m_p^*}{m_p}\right)^4\left(\frac{n_p}{n_0}\right)^{1/3}\mathcal{N}_\nu\, T_9^8\,\mathrm{erg\,cm^{-3}\,s^{-1}} \\ Q_\nu^{np} =& 1.05\times10^{20}\left(\frac{m_n^* m_p^*}{m_n m_p}\right)^2\left(\frac{n_p}{n_0}\right)^{1/3}\mathcal{N}_\nu T_9^8\,\mathrm{erg\,cm^{-3}\,s^{-1}} \end{aligned} \tag{2.15}$$

where $\mathcal{N}_\nu = 3$ is the number of neutrino flavours. All three bremsstrahlung processes are of comparable intensity, with $Q_\nu^{pp} < Q_\nu^{np} < Q_\nu^{nn}$. The neutrino bremsstrahlung has the same dependence $\propto T^8$ of the mUrca processes, but the coefficient is about two orders of magnitude less. Thus, in normal conditions it is almost negligible, but it can be the most important neutrino process in presence of nucleon superfluidity suppressing the mUrca emissivity.

The presence of muons does affect neutrino bremsstrahlung, but it can be greatly enhanced near the threshold of appearance of the reacting hyperons. This is because in the vicinity of the threshold the number density of the hyperons is so small that the particles are yet non-degenerate, and reactions like

$$\Sigma^-\Sigma^- \to \Sigma^-\Sigma^-\nu\bar{\nu}$$

do not suffer the strong suppression of the emissivity associated with the degeneracy. However, such an enhancement occurs only in very thin layers of neutron star cores and seems to have no effect on the total neutrino luminosity.

Quark matter It has been speculated for some decades [Wit84] that in the inner core of a NS quark deconfinement can take place. In such a scenario, the quark analogous of the aforementioned weak processes can take place. Since u and d quarks are to be considered ultra–relativistic and for the character of strong force itself there is no kinematic threshold [Iwa82]. Therefore, the leading process is analogous to direct Urca,

$$\begin{cases} u\ l \to d\ \nu_l \\ d \to u\ l\ \bar{\nu}_l \end{cases} \tag{2.16}$$

and its emissivity can be calculated in an analogous way, with the difference that the phase space allowed by strong force is smaller. The result is [Iwa82]

$$Q = \frac{914 G_F^2 \cos^2\theta_C}{315\hbar^{10}c^6} \alpha_c p_F^d p_F^u p_F^e k_b^6 T^6 \simeq (10^{23} - 10^{24})\, T_9^6 \mathrm{erg\,cm^{-3}\,s^{-1}} \tag{2.17}$$

where G_F is Fermi constant, θ_C is the Cabibbo angle and α_c is the strong force adimensional coupling. The numerical expression is given only as an order–of–magnitude value because of the rather high theoretical uncertainty on the (small) value that the strong coupling α_c should assume in this context [DSW83]. Aside, quark modified Urca and bremsstrahlung processes are still present, but of negligible intensity.

In addition, some models predict the appearance of free strange quarks whose role seems to be less important for NS cooling. Since they are more massive they must be considered non–relativistic, and this produces lower emissivities [Iwa82].

Plasma processes in the crust In the crust matter is composed by ordinary atoms, and the main contribution to neutrino emission comes from electrons. A great variety of processes can happen, and the whole physics of the crust is not well understood as yet. However, crustal neutrino emission is dominated by *plasmon decay*, and considering this process only is enough for most purposes. Due to energy–momentum conservation, a single electron cannot emit a neutrino pair. This process, though, becomes possible if the electron is surrounded by a medium with which it can interact, so gaining the required energy for the process $e \to e\ \nu\ \bar{\nu}$. This process is usually written as

$$\tilde{\gamma} \to \nu\bar{\nu} \tag{2.18}$$

where $\tilde{\gamma}$ stands for a plasmon. This process can produce neutrinos of any flavour; since different types of plasmon can appear, their emissivites must be summed. The total emissivity is obtained performing the integrals in eq. (2.6) using dispersion relations from standard plasma theory,

$$\omega_l^2 = \omega_p^2 + \frac{3}{5}k^2c^2 \qquad \omega_t^2 = \omega_p^2 + \frac{6}{5}k^2c^2 \tag{2.19}$$

where l labels a longitudinal plasmon, t a transverse one and the plasma frequency $\omega_p = \sqrt{4\pi e^2 n_e / m_e^*}$ has been introduced. These expression are valid in the limit of ultrarelativistic degenerate electrons, while in the opposite case longitudinal plasmons are suppressed by strong Landau damping and transverse ones are reduced to ordinary e.m. waves unaffected by the medium. The emissivity is

$$Q_{pl} = 1.39 \times 10^{21} I_{pl} \mathrm{erg\,cm^{-3}\,s^{-1}} \tag{2.20}$$

where $I_{pl} = I_l + I_t$ is the sum of two integrals that must be evaluated numerically. Their value is exponentially suppressed for low temperatures, while in the high–temperature limit, $kT \gg \omega_p$, they are given by [BS93]

$$I_t = 16.23 \frac{T^3 \omega_p^6}{m_e^9} \qquad I_l = 0.349 \frac{T \omega_p^8}{m_e^9} \tag{2.21}$$

so that the leading contribution comes from transverse plasmons, which have a larger phase space. Since $\omega_p \propto \rho^{1/3}$, emissivity strongly depends on density. It reaches a maximum for $\omega_p \approx T$, which for a NS is a very high value: for example, $\omega_p \simeq 1.5\,\mathrm{MeV}$ at neutron drip ($\rho \simeq 4.4 \times 10^{11}\,\mathrm{g\,cm^{-3}}$). Hence, plasmon decay is an efficient process at very high temperatures, i.e., in the very early stages of NS cooling when it can be the overall dominant one, while it becomes unimportant in later stages.

2.4 Transparency to neutrinos

Throughout this work, matter is considered completely transparent to neutrinos. This fact has already been introduced, since we neglected the neutrino distribution function in the emissivity of the processes described in the previous section. In cooling simulation, no heating terms due to neutrino absorption will be considered. Neutrinos can interact with other particles only via charged or neutral weak currents. Considering electrons, the cross section of the process is [ST83]

$$\sigma_e \simeq \left(\frac{\hbar}{m_e c}\right)^{-4} \left(\frac{G_F}{m_e c^2}\right)^2 E_\nu \frac{E_\nu^2}{E_F^e} \approx \left(\frac{100\,\mathrm{keV}}{E_\nu}\right) 10^{-44}\,\mathrm{cm^2} = \left(\frac{100\mathrm{keV}}{E_\nu}\right) 10\,\mathrm{zb} \tag{2.22}$$

where the term involving electron Fermi energy E_F^e takes into account electron degeneracy. Thus the mean free path of a neutrino before scattering onto an electron is ($n_e \approx (\rho/\rho_0)^2$)

$$\lambda_e = \frac{1}{\sigma_e n_e} \simeq 9 \times 10^7\,\mathrm{km} \left(\frac{\rho_0}{\rho}\right)^{4/3} \left(\frac{100\,\mathrm{keV}}{E_\nu}\right)^3 \tag{2.23}$$

which is much higher than the typical NS radius, $R \approx 10\,\mathrm{km}$.

Neutrinos can also scatter, only via neutral current, with neutrons. The cross section of the process is

$$\sigma_n = (G_F \cos\theta_C)^2 E_\nu^2 \approx 9 \times 10^{-46}\,\mathrm{cm}^2 \left(\frac{E_\nu}{100\mathrm{keV}}\right)^2 = 0.9 \left(\frac{E_\nu}{100\mathrm{keV}}\right)^2 \mathrm{zb}. \tag{2.24}$$

This value is much lower than the electron cross section, since there is no contribution from charged current interactions. Then, the mean free path is

$$\lambda_n = \frac{1}{\sigma_n n_n} \simeq 300\,\mathrm{km} \frac{\rho_0}{\rho} \left(\frac{100\,\mathrm{keV}}{E_\nu}\right)^2. \tag{2.25}$$

The effective mean free path of neutrinos can be estimated as the geoometric mean of the two,

$$\lambda_{\mathrm{eff}} = \sqrt{\lambda_e \lambda_n} \simeq 2 \times 10^5\,\mathrm{km} \left(\frac{\rho_0}{\rho}\right)^{7/6} \left(\frac{100\,\mathrm{keV}}{E_\nu}\right)^{5/2} \tag{2.26}$$

which, although is not as high as the electron value, is still much larger than the NS radius. Therefore, the assumption of transparency to neutrinos is valid.

2.5 Superfluidity

Consider a system, say a fluid, of quantum (quasi)particles at absolute zero temperature and let they have an elementary excitation dispersion relation $\varepsilon(p)$. If $\varepsilon(0) \equiv \Delta \neq 0$ the system exhibits the phenomenon of *superfluidity*. In fact, if the fluid moves too slowly to fill this energy gap no excitation can appear and the motion goes on without energy transfer, i.e., with no dissipation. For $T \neq 0$, a boson system behaves like the mixture of two fluids, one undergoing normal dissipative motion and a superfluid one. The ratio between the two fluids depend on the temperature, and eventually superfluid (SF) behaviour vanishes above a critical temperature T_c.

Such a behaviour is not expected to show up in fermion systems. However, the manifestation of superfluidity is possible also in fermion systems with mutual attraction through the BCS mechanism [BCS57]: it is energetically favourable for fermions to join, forming *Cooper pairs* of bosonic nature. Near $p = 0$, the energy spectrum of this system is [LLP77]

$$\varepsilon(p) = \sqrt{\Delta^2 + \eta_p^2} \tag{2.27}$$

where $\eta_p = p^2/2m - \mu$ and $\Delta \propto \exp(-2\pi^2\hbar^3/gmp_F)$ being g the effective coupling constant of the attraction. Then, $\varepsilon(0) = \Delta \neq 0$ and superfluidity arises.

		D [MeV]	κ_0 [fm^{-1}]	κ_1 [fm^{-2}]	κ_2 [fm^{-1}]	κ_3 [fm^{-2}]	γ
p	$^1S_0$	120	0	9	1.3	1.8	1.764
n	$^1S_0$	68	0.1	4	1.7	4	
n	$^3P_2$	0.15	2	0.1	3.1	0.02	1.188

Table 2.3: Phenomenological parameters from equations 2.28 and 2.29.

Superfluidity in nuclear matter is a crucial element in NS cooling. However, the details of nucleon interactions are not well understood yet, so the types of pairing appearing in the ground state of nuclear matter are not known. In particular, nucleon pairing can occour in states with different angular momentum. Using a spectroscopic–like notation, they are $^1S_0$ and $^3P_2$. Moreover, the $^3P_2$ pairing can come with three values for the projection of spin along the quantizing axis, $m_z = 0$ or $m_z = \pm 2$. The ground state of nuclear matter probably is given by a mixture of these states.

The value of critical temperature T_c is not known in detail. Following [KHY01] and references therein, introducing the wavenumber $k = (3\pi^2 n)^{1/3}$, the zero–temperature energy gap can be parametrized as

$$\Delta_0 = D \frac{(k-\kappa_0)^2}{(k-\kappa_0)^2+\kappa_1} \frac{(k-\kappa_2)^2}{(k-\kappa_2)^2+\kappa_3} \tag{2.28}$$

where T_0 and the κ's were computed in [HN12] in order to explain the cooling data of Vela and Geminga PSRs. Their values are found in table 2.3. Then, the critical temperature is found as

$$T_c = \frac{\Delta_0}{k_B \gamma} \tag{2.29}$$

where γ is a phenomenological parameter depending on pairing type. The dependence of T_c is shown in fig. 2.4.

At $T \neq 0$, the SF gap can be factorized as $\Delta(T)F(\theta)$, where the function F depends on superfluidity type and $\Delta(T)$ is given by the BCS equation,

$$\log\left[\frac{\Delta_0}{\Delta(T)}\right] = 2\lambda \int \frac{\mathrm{d}\Omega}{4\pi} \int_0^\infty \frac{\mathrm{d}x}{z} f(z) F(\theta) \tag{2.30}$$

where λ is a numerical coefficient and

$$z = \frac{\varepsilon - \mu}{k_B T} \qquad x = \frac{\eta}{k_B T}.$$

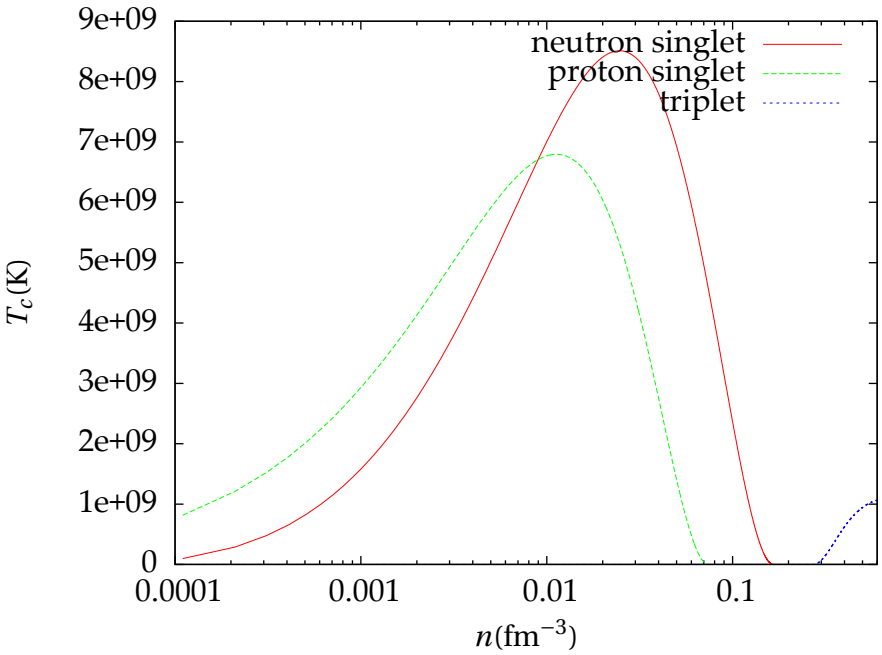

Figure 2.4: Critical temperature for the SF transition.

This produces values $\Delta \approx 0.1 - 1\,\text{MeV}$. It is convenient to introduce the adimensional variables

$$v = \frac{\Delta(T)}{k_B T} \qquad \tau = \frac{T}{T_c} \tag{2.31}$$

so that for our three SF types the solutions of BCS equation can be expressed with simple fits, [YGH01]

$$\begin{aligned} v_A &= \sqrt{1-\tau}\left(1.456 - \frac{0.157}{\sqrt{\tau}} + \frac{1.764}{\tau}\right) \\ v_B &= \sqrt{1-\tau}\left(0.7893 + \frac{1.188}{\tau}\right) \\ v_C &= \frac{\sqrt{1-\tau^4}}{\tau}\left(2.030 - 0.4903\tau^4 + 0.1727\tau^8\right) \end{aligned} \tag{2.32}$$

which will be useful in evaluating the effects of SF phases. Here and in the following, subscript A indicates the singlet state, B the triplet with $|m_z| = 0$ and C the triplet state with $|m_z| = 2$.

The appearance of a SF phase has two main consequences on cooling processes: the reaction rates of neutrino processes are modified and new reactions open.

Reaction rates are altered since superfluidity modifies the dispersion relation that must be used when performing phase–space integrals. In general, this can be taken into account by the use of a *superfluid reduction factor* $\mathfrak{R}$,

$$Q_\nu = \mathfrak{R} Q_\nu^{\text{non–SF}} \tag{2.33}$$

which is given by the ratio

$$\mathfrak{R} = \frac{\int \prod_i \mathrm{d}\Omega_i \int_0^\infty \mathrm{d}x_\nu\, x_\nu^3 \left(\prod_i \int_{-\infty}^{+\infty} \mathrm{d}x_i f(z_i)\right) \delta^{(1)}\left(x_\nu - \sum_i z_i\right) \delta^{(3)}\left(\sum_i p_i\right)}{\int \prod_i \mathrm{d}\Omega_i \int_0^\infty \mathrm{d}x_\nu\, x_\nu^3 \left(\prod_i \int_{-\infty}^{+\infty} \mathrm{d}x_i f(x_i)\right) \delta^{(1)}\left(x_\nu - \sum_i x_i\right) \delta^{(3)}\left(\sum_i p_i\right)} \tag{2.34}$$

where x is the reduced Fermi momentum and $z = \varepsilon(p)/k_B T$; for non–SF particles, $z = x$. The denominator of this expression is the quantity involved in the phase–space integration of 2.6 for the non–SF case. If only one nucleon is SF, $\mathfrak{R}$ depends only on the gap υ. Reduction factors for the relevant processes in NS cooling were first computed by [LY94] using a fit to values obtained numerically,

$$\begin{aligned}
\mathfrak{R}_A^D(\upsilon) &= \left[0.2312 + \sqrt{(0.7688)^2 + (0.1438\upsilon)^2}\right]^{5.5} \exp\left(3.427 - \sqrt{(3.427)^2 + \upsilon^2}\right) \\
\mathfrak{R}_B^D(\upsilon) &= \left[0.2546 + \sqrt{(0.7454)^2 + (0.1284\upsilon)^2}\right]^{5} \exp\left(2.701 - \sqrt{(2.701)^2 + \upsilon^2}\right) \\
\mathfrak{R}_C^D(\upsilon) &= \frac{0.5 + (0.09226\upsilon)^2}{1 + (0.1821\upsilon)^2 + (0.16736\upsilon)^4} + \frac{1}{2}\exp\left(1 - \sqrt{1 + (0.4129\upsilon)^2}\right)
\end{aligned} \tag{2.35}$$

showing that emissivities are exponentially suppressed for strong superfluidity ($T \gg T_c$).

Reduction factors for modified Urca processes are computed in a similar fashion. From the definition, one can easily see that in the singlet state (i.e., no angular integrals) the proton branch reduction factor for a SF neutron $\mathfrak{R}_n^{mp}$ is the same as the one for the neutron branch with a SF proton $\mathfrak{R}_p^{mn}$ and viceversa, $\mathfrak{R}_n^{mn} = \mathfrak{R}_p^{mp}$. Convenient fits are

$$\begin{aligned}
\mathfrak{R}_{nA}^{mp} \equiv \mathfrak{R}_{pA}^{mn} &= \frac{a^{5.5} + b^{7.5}}{2} \exp\left(3.4370 - \sqrt{(3.4370)^2 + \upsilon^2}\right) \\
a &= 0.1477 + \sqrt{(0.8523)^2 + (0.1175\upsilon)^2}; \qquad b = 0.1477 + \sqrt{(0.8523)^2 + (0.1297\upsilon)^2} \\
\mathfrak{R}_{nA}^{mn} \equiv \mathfrak{R}_{pA}^{mp} &= \left[0.2414 + \sqrt{(0.7586)^2 + (0.1318\upsilon)^2}\right]^{7} \exp\left(5.339 - \sqrt{(5.339)^2 + (2\upsilon)^2}\right).
\end{aligned} \tag{2.36}$$

Triplet state factors are much harder to compute: for the proton branch an expression is known, while for the neutron branch it is necessary to use an

approximation:

$$\begin{aligned}
&\mathfrak{R}_{nB}^{mp} = \frac{a^7 + b^5}{2} \exp\left(2.398 - \sqrt{(2.398)^2 + v^2}\right) \\
&\quad a = 0.1612 + \sqrt{(0.8388)^2 + (0.1117\,v)^2}; \qquad b = 0.1612 + \sqrt{(0.8388)^2 + (0.1274\,v)^2} \\
&\mathfrak{R}_{nB}^{mn} \approx \mathfrak{R}_{pA}^{mp}(v_n).
\end{aligned} \tag{2.37}$$

The reduction factors for C type SF is not interesting for our purposes, since it is triggered in regimes in which modified Urca is not relevant.

For reactions involving two SF nucleons, the integrals in eq. (2.34) become very complicated. However, for the accuracy required in NS cooling reduction factors can be estimated through the approximate relations

$$\begin{aligned}
\mathfrak{R}_{IJ}^{D} &\simeq \min\left(\mathfrak{R}_{I}^{D}, \mathfrak{R}_{J}^{D}\right) \\
\mathfrak{R}_{BA}^{Mp}(v_n, v_p) &\simeq \frac{\mathfrak{R}_{BA}^{D}(v_n, 2v_p)}{\mathfrak{R}_{B}^{D}(v_n)} \mathfrak{R}_{B}^{Mp}(v_n) \\
\mathfrak{R}_{BA}^{Mn}(v_n, v_p) &\simeq \frac{\mathfrak{R}_{BA}^{D}(2v_n, v_p)}{\mathfrak{R}_{A}^{D}(v_p)} \mathfrak{R}_{A}^{Mn}(v_p).
\end{aligned} \tag{2.38}$$

As to new reactions, the appearance of the energy gap δ allows the processes

$$B \to B\ \nu_i\ \bar{\nu}_i$$

where B stands for any baryon (nucleons but also hyperons) and i labels any of the three lepton flavours. In normal conditions, this process is forbidden by energy–momentum conservation, but the energy from the gap $\varepsilon(0) \neq 0$ can be used to overcome it. The corresponding neutrino emissivity Q_ν^{sf} is

$$Q_\nu^{\mathrm{sf}} = F(\tau) 1.17 \times 10^{21} \left(\frac{m_B^*}{m_B}\right) \left(\frac{p_F}{m_B c}\right) T_9^7\, a_B \mathcal{N}_\nu \mathrm{erg\,cm^{-3}\,s^{-1}} \tag{2.39}$$

where $F(\tau)$ is a function depending on pairing type that is exponentially suppressed for $T > T_c$[†], a_B is a weak interaction effective constant depending on nucleon species and pairing type and $\mathcal{N}_\nu = 3$ is the number of lepton flavours.

Note that since SF behaviour is significant only near the Fermi surface, it will not change the bulk properties of matter. This implies that the hydrostatic structure of the object is not affected by SF phases.

[†]See [YGH01] for convenient numerical expressions.

2.6 Specific heat and thermal conductivity

For a gas of degenerate fermions of number density n the specific heat is [Vig13]

$$c_v = \pi^2 \frac{n k_B^2 T}{m c^2} \frac{\sqrt{x_F^2 + 1}}{x_F^2}. \tag{2.40}$$

For electrons in the NS c_v can be evaluated in the ultrarelativistic limit,

$$c_v^e \simeq 5.4 \times 10^{19} \left(\frac{n_e}{n_0}\right)^{2/3} T_9 \,\mathrm{erg\,cm^{-3}\,K^{-1}} \tag{2.41}$$

while for nucleons ($N = n, p$) it takes the non relativistic value,

$$c_v^N \simeq 1.6 \times 10^{20} \frac{m_N^*}{m_N} \left(\frac{n_N}{n_0}\right)^{1/3} T_9 \,\mathfrak{R}^{cv} \,\mathrm{erg\,cm^{-3}\,K^{-1}} \tag{2.42}$$

where $n_0 = 0.16\,\mathrm{fm}^{-3}$ is the nuclear saturation number density and $\mathfrak{R}^{cv}$ suppresses specific heat in presence of superfluidity. Numerical calculations of these factors are well fitted by the expressions [LY94]

$$\begin{aligned}
\mathfrak{R}_A^{cv} &= \left(0.4186 + \sqrt{(1.007)^2 + (0.5010\,v)^2}\right)^{2.5} \exp\left(1.456 - \sqrt{(1.456)^2 + v^2}\right) \\
\mathfrak{R}_B^{cv} &= \left(0.6893 + \sqrt{(0.790)^2 + (0.2824\,v)^2}\right)^{2} \exp\left(1.934 - \sqrt{(1.934)^2 + v^2}\right) \\
\mathfrak{R}_C^{cv} &= \frac{2.188 - (9.537 \times 10^{-5})^2 + (0.1491\,v)^4}{1 + (0.2846\,v)^2 + (0.01335\,v)^4 + (0.1815\,v)^6}
\end{aligned} \tag{2.43}$$

for the three types of superfluidity.

Assuming NS matter to be isotropic, i.e., neglecting magnetic fields and solid state effects, the heat conductivity tensor reduces to a constant, $\kappa_{ij} = \kappa \delta_{ij}$. Thermal conduction in a NS core is due to neutrons, since they are by far the most abundant particles, and leptons, since they do not experience strong forces and thus have a larger mean free path. The thermal conductivity of protons is negligible [FI79]. Moreover, neutron and lepton conductions are due to different (nuclear or Coulomb) forces, so that they can be studied separately. In general, κ depends on the characteristic relaxation times of the interactions, to be computed via a system of Boltzmann equations. Neutron conduction was studied in [BHY01] using the Landau–Fermi theory of fermion liquids. The resulting expression is

$$\kappa_n \simeq 7.2 \times 10^{23} T_8 \,\mathfrak{R}_\kappa^2(\Delta_n) \left(\frac{m_n}{m_n^*}\right) \left(\frac{10^{15}\,\mathrm{Hz}}{\nu_{nn} + \nu_{np}}\right) \left(\frac{n_n}{n_0}\right) \mathrm{erg\,cm^{-1}\,s^{-1}\,K^{-1}} \tag{2.44}$$

where $\mathfrak{R}_\kappa(\Delta_n)$ is a SF reduction factor, T_8 is the temperature in units of 10^8 K and ν_{ab} is the characteristic frequency of interaction between particles a and b. The relevant frequencies are given by

$$\begin{aligned}\nu_{nn} &\simeq 3.48\times 10^{15}\left(\frac{m_n^*}{m_n}\right)^3 T_8^2\,\mathfrak{F}_1\,\mathrm{Hz}\\ \nu_{np} &\simeq 3.48\times 10^{15}\left(\frac{m_n^*}{m_n}\right)\left(\frac{m_p^*}{m_p}\right)^2 T_8^2\,\mathfrak{F}_2\,\mathrm{Hz}\end{aligned} \tag{2.45}$$

where $\mathfrak{F}_1$ and $\mathfrak{F}_2$ are functions taking account of superfluid effects ‡. Note that these frequencies are proportional to T^2. Therefore the thermal conductivity depends on temperature as $\kappa \propto T^{-1}$. This is a general feature of highly degenerate (non–SF) particles.

The electron contribution was studied analogously in [GY95]. The main differences are the ultrarelativistic conditions and the fact that the interaction involved is the electromagnetic one. Thermal conduction is given by ee and ep interactions. In normal conditions, the latter dominates and

$$\kappa_e \simeq 6.3\times 10^{24}\frac{C}{T_8}\left(\frac{m_p}{m_p^*}\right)^{1/2}\left(\frac{n_e}{n_0}\right)^{7/6}\mathrm{erg\,cm^{-1}\,s^{-1}\,K^{-1}} \tag{2.46}$$

where $C \simeq 1.2$ is a charge screening parameter. Since $n_e \propto \rho^2$ in a npe NS core, $\kappa_e \propto \rho^{7/3}$. Conversely, if protons are in SF phase scattering is suppressed, and the dominant part is the ee one,

$$\kappa_e \simeq 4.3\times 10^{24}\frac{C}{T_8}\left(\frac{n_e}{n_0}\right)\mathrm{erg\,cm^{-1}\,s^{-1}\,K^{-1}} \tag{2.47}$$

and in this case $\kappa_e \propto \rho^2$. Generally, this value is smaller than the non SF one of 1–2 orders of magnitude. Near T_c, both effects must be considered.

‡See [BHY01] for convenient fitted expressions for $\mathfrak{R}_\kappa$ and $\mathfrak{F}$

3 | Solving the Structure Equations

The first step to investigate NS cooling is to solve the structure equations of the star. This has been done providing an EoSs and solving the hydrostatic equilibrium problem. Since all reactions occour for particles near the Fermi sphere, the bulk properties of degenerate matter are not affected by the thermal evolution. Therefore, the hydrostatic structure is to be kept fixed during the NS evolution.

3.1 TOV integration

As described in more detail in section 1.4, the GR hydrostatic equilibium is described by the equations

$$\begin{aligned}
\frac{\mathrm{d}p}{\mathrm{d}r} &= -\frac{GM(r)\rho}{r^2}\left(1+\frac{p(r)}{\rho c^2}\right)\mathscr{G}\mathscr{V}^2 \\
\frac{\mathrm{d}M}{\mathrm{d}r} &= 4\pi r^2 \rho(r) \\
\frac{\mathrm{d}\Phi}{\mathrm{d}r} &= -\frac{\mathrm{d}p}{\mathrm{d}r}\left(\frac{1}{p(r)+\rho(r)c^2}\right) \\
\frac{\mathrm{d}a_b}{\mathrm{d}r} &= 4\pi r^2 n_b \left(1-\frac{2GM(r)}{rc^2}\right)^{-1/2} \qquad \rho(r) = a_b(r) m_b
\end{aligned} \tag{3.1}$$

which must be integrated with the conditions

$$M(0) = 0 \qquad p(0) = p_c \qquad \Phi(R) = \frac{1}{2}\log\left(1-\frac{2GM_{tot}}{Rc^2}\right). \tag{3.2}$$

Two of these conditions provide initial values, while the third is a boundary condition; nevertheless, the whole set of equations can be treated as an initial value problem. In fact, the equation for Φ is homogeneous, and thus it can be solved imposing an arbitrary initial value $\Phi(0)$ and then adding a global offset to match the boundary condition once radius $r = R$ is reached.

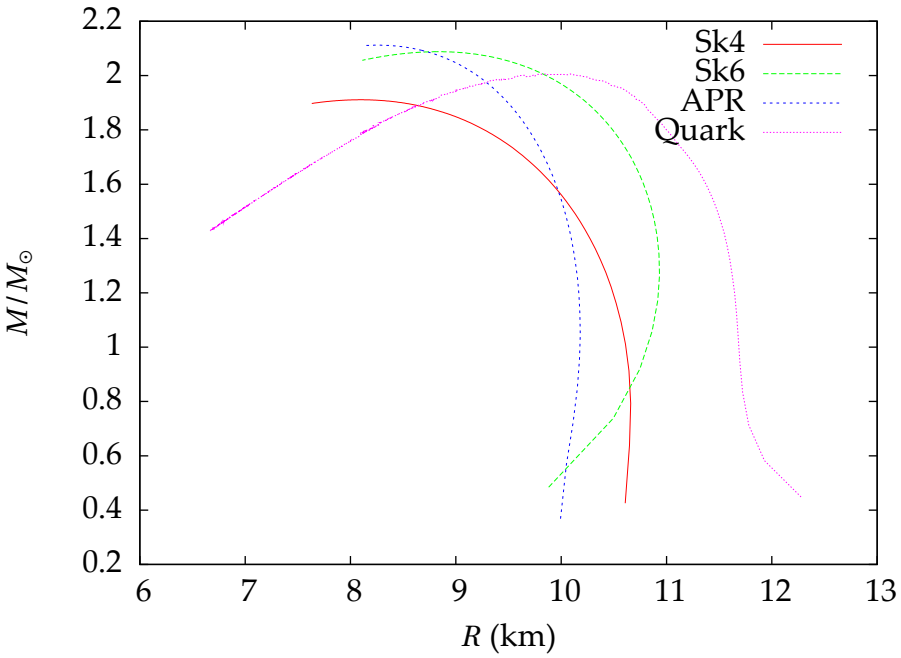

Figure 3.1: Mass–radius relation.

The relation between the initial conditions, in particular central pressure, and the total radius is not known *a priori*, therefore the ODEs have been solved on an interval greater than the typical expected radius ($R_{\max} = 20\,\mathrm{km}$ while expected radii are $\approx 10\,\mathrm{km}$) and the total radius was determined through the condition $p(R) = 0$. The system of ODEs has been solved using the finite difference method described in [NT88].

The widest range for the central pressure p_c compatible with each EoS has been scanned, building several NS models. This procedure produces the pressure, density and chemical composition profile of single stars as well as the relations between the total mass and radius and total mass and central density for the whole set of NSs built from the given EoS.

In fig. 3.1 and fig. 3.2, the M–R and M–ρ_c relations are presented. An important feature of these relations is the presence of a maximum value for the mass of a gravitationally bound object. This is a typically general–relativistic property, associated with the form of TOV equation. Figure 3.3 shows the M–ρ_c relation for APR EoS with dots corresponding to models of NSs with linearly increasing central pressure, $\Delta p_c = 1.4 \times 10^{34}\,\mathrm{MeV\,fm^{-3}}$. The point corresponding to the maximum mass acts as an accumulation point for them. Then, the curve stops, and points beyond the maximum mass correspond to unbound solutions. The maximum mass values are in a range $1M_\odot \lesssim M_M \lesssim 2M_\odot$, see 3.2.

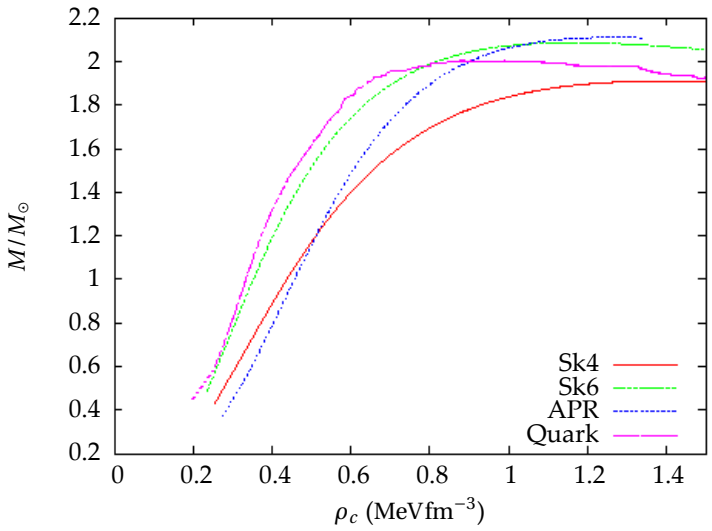

EoS	$M_{\max}/M\odot$
Sk4	1.98
Sk6	2.16
APR	2.18
Quark	2.01

Figure 3.2: Central density–Mass relation.

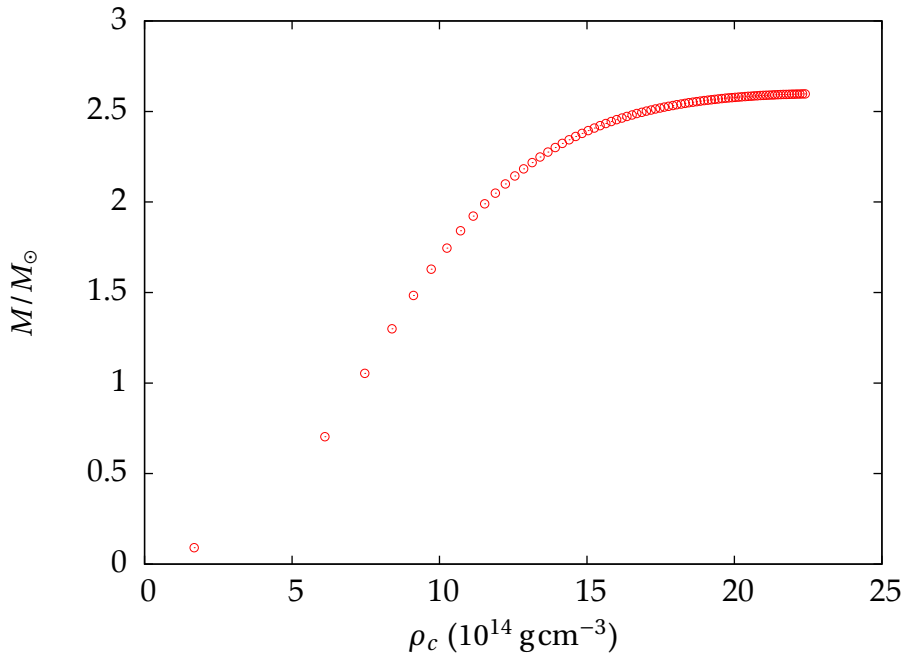

Figure 3.3: Mass–central density relation. Dots correspond to NS models separated by a constant difference in the central pressure. The maximal mass point acts as an accumulation point.

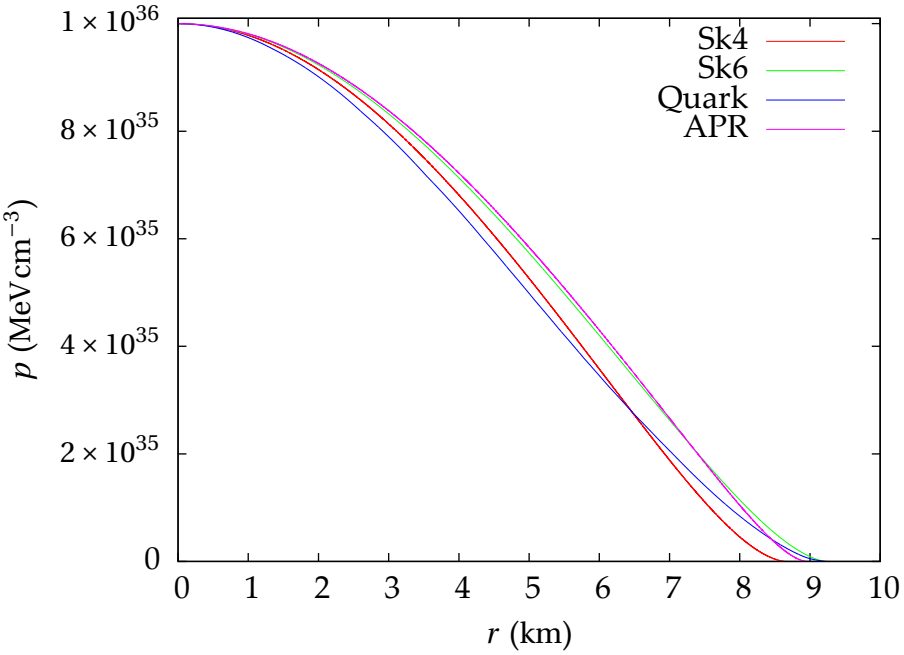

Figure 3.4: Different solutions of TOV equation for the same initial conditions with different EoSs.

As a result, some EoSs can be ruled out already at this stage, since it has been observed a NS, the pulsar J1614–2230, with $M = (1.97 \pm 0.04) M_\odot$ [DP+10]. This puts a very tough constraint on EoSs involving exotic particles. In general, not all the EoSs do include the details of the condensed state of matter in the outer crust (as a general rule, the crust begins when $\rho \simeq \rho_{cc} = 1.5 \times 10^{14}\,\mathrm{g\,cm^{-3}}$). However, the obtained results are not substantially flawed by this, since the liquid core cover almost the 99% of the NS mass. All the EoSs of our case predict a maximum mass value compatible with this observation even though the Sk4 equation predicts a maximum mass value of $1.98 M_\odot$, which would imply that J1614–2230 is an object very close to instability.

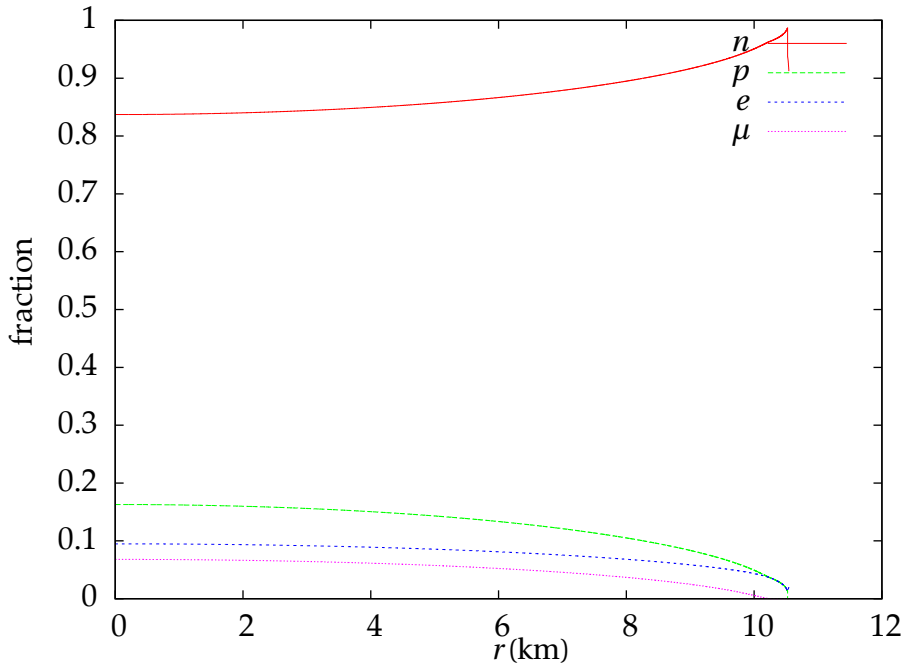

Figure 3.5: Example of chemical composition for a star of $M = 1.77 M_\odot$ with Sk4 EoS.

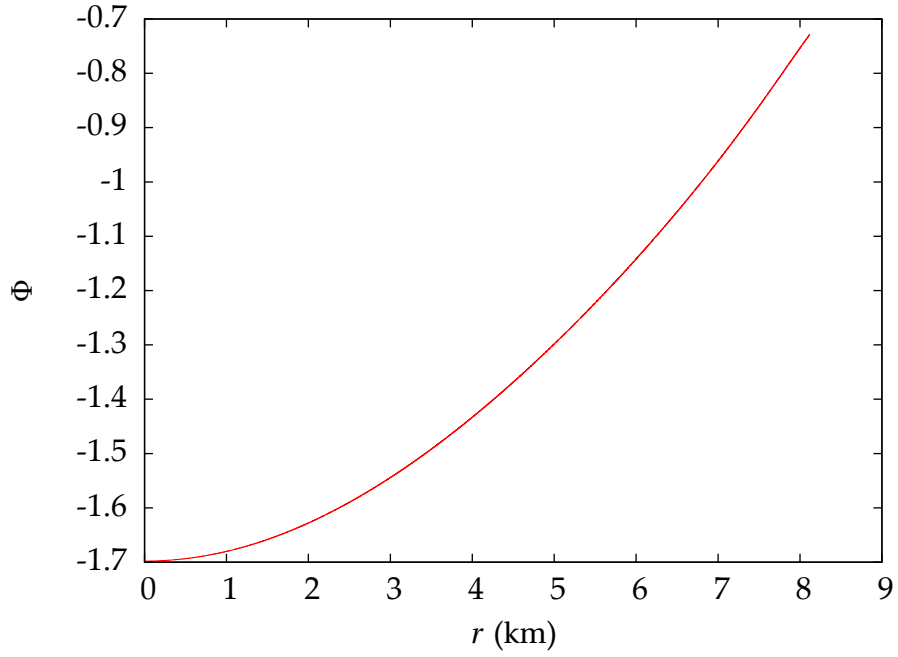

Figure 3.6: Radial profile of Φ for a $1.1 M_\odot$ star with APR EoS.

4 | Cooling of non–SF NSs

Once the hydrostatic structure of a NS is determined, the processes described in chapter 2 can be exploited to follow the cooling history of the object. Since the degeneracy of the great number of parameters involved in the problem is huge, we will concentrate on the APR EoS only. The effects of superfluidity are neglected for the moment, and will be studied in next chapter.

4.1 Analytical solutions: Fast and Slow cooling

Of course, finding an exact analytic solution of eq. (2.1) for realistic EoS and emissivities is impossible. However, an analytical treatment is possible introducing some very rough approximations. In particular, we can isolate the temperature dependence only in our quantities,

$$c_v = CT \qquad L_\nu = NT^k \qquad L_\gamma = PT_e^4 \tag{4.1}$$

for constant C, N and P. This means neglecting the radial dependences (i.e., density dependence) of the quantities; $k = 6$ for dUrca processes, $k = 8$ for all the others. This allows one to integrate over the radius, obtaining the simpler equation

$$c_v \frac{\mathrm{d}T}{\mathrm{d}t} = -L_\nu - L_\gamma \tag{4.2}$$

where also GR effects where neglected. In the case of pure neutrino cooling, corresponding to the first stages of evolution, the equation reads

$$\frac{\mathrm{d}T}{\mathrm{d}t} = -\frac{N}{C} T^{k-1} \quad \Longrightarrow \quad \begin{cases} T \sim t^{-1/6} & \text{mUrca} \\ T \sim t^{-1/4} & \text{dUrca} \end{cases} \tag{4.3}$$

where the two possible values of k depending on the presence of direct Urca processes give rise to two different cooling scenarios: *fast cooling* if direct process is allowed, *slow cooling* if only modified ones occour.

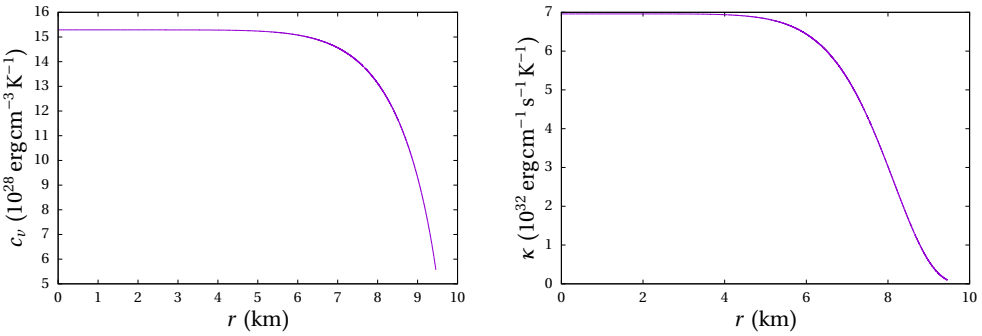

(a) *Radial profile of specific heat.* (b) *Radial profile of thermal conductivity.*

Figure 4.1: Radial profile of transport properties (APR EoS).

From an historical point of view, fast cooling was the first scenario to be proposed in a landmark paper by G. Gamow [GS41], that was the first to consider neutrinos as a significant energy loss channel for stars. However, it was soon realized that fast cooling is not compatible with observations, since it would drain the whole energy of a NS in few centuries. Therefore, higher order processes were to be introduced in order to explain the observed temperatures, i.e., the slow cooling scenario.

In the case of pure photon cooling, describing the latter stages of the star evolution, we have a black body emission depending on the effective surface temperature T_e. This can be related to the core temperature by eq. (2.5), that can be rewritten schematically as $T_e \sim T^{1/2+\alpha}$ with $\alpha \approx 1/8$. Hence, during the photon dominated era cooling goes like

$$\frac{\mathrm{d}T}{\mathrm{d}t} = -\frac{P}{C} T^{1+4\alpha} \quad \Longrightarrow \quad T \sim t^{-\frac{1}{4\alpha}}. \tag{4.4}$$

Therefore, a knee in the cooling curve is expected when photon cooling takes over the neutrino one.

Neglecting radial dependences may appear too great a simplification, but it is justified by the fact that in the first stages of the NS life the main effect is the isothermalization of the core. Figure 4.2 shows the cooling curves obtained for one cooling process only in isothermal approximation; coefficients were calculated by integration,

$$CT = \int_0^R \mathrm{d}V c_v \qquad NT^8 = \int_0^R \mathrm{d}V Q_\nu \qquad PT^4 = \int_0^R \mathrm{d}V Q_\gamma \tag{4.5}$$

in order to have realistic values. The behaviour is in both cases, as expected, a power law decay following a plateau. This begins in $t \sim 100\,\mathrm{y}$ for neutrinos, in

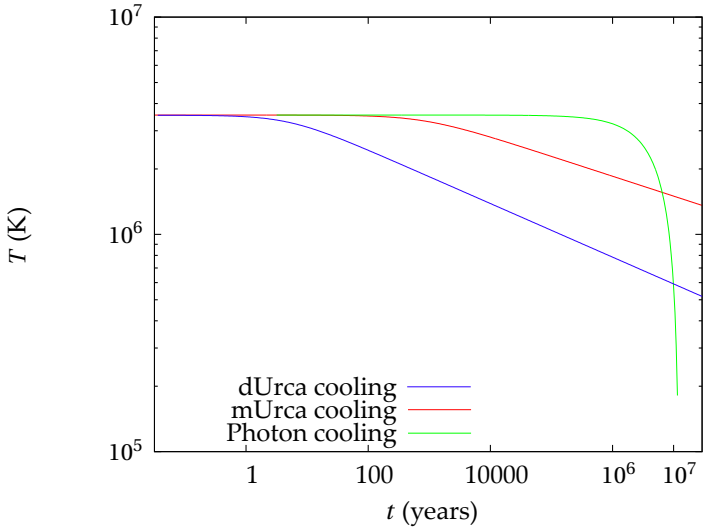

Figure 4.2: Simplified cooling curves for completely isothermal stars.

$t \sim 10^6$y for photons. In next section this will be compared with the complete model.

4.2 Cooling curves

The system of eq. (2.3) has been solved numerically using a completely implicit integration scheme based on Newton–Raphson method. To reduce the number of operations, the equations were rewritten using the baryon number instead of the radius as the independent variable: according to eq. (1.23) they are related by

$$\mathrm{d}a = 4\pi r^2 n_b \mathscr{V}\,\mathrm{d}r \tag{4.6}$$

so that the system to be solved can be expressed as

$$\begin{cases} \dfrac{\partial \mathscr{T}}{\partial t} + \mathscr{R}^2 \dfrac{Q_\nu}{c_\nu} + \dfrac{n_b}{c_\nu}\dfrac{\partial \mathscr{L}}{\partial a} \equiv F_a = 0 \\ \mathscr{L} + \kappa(4\pi r^2)^2 n_b \mathscr{R} \dfrac{\partial \mathscr{T}}{\partial a} \equiv F_b = 0 \end{cases} \tag{4.7}$$

(notation as in eq. (2.3)) with the boundary conditions

$$L(t, r=0) = 0 \qquad L(t, r=R) = 4\pi R^2 \sigma \left(T_s(T_b)\right)^4$$

where the latter is obtained using the T_s–T_b relation of eq. (2.5).

The system of 2 PDEs is discretized on a space–time grid of $N \times N$ elements and written as a set of $2N$ algebraic equations,

$$\vec{F}(\vec{X}) = 0, \quad \text{with} \quad \vec{X} = \begin{pmatrix} \mathscr{L}(r_1) \\ \mathscr{T}(r_1) \\ \vdots \\ \mathscr{L}(r_N) \\ \mathscr{T}(r_N) \end{pmatrix} \quad \text{and} \quad \vec{F} = \begin{pmatrix} F_a(r_1) \\ F_b(r_1) \\ \vdots \\ F_a(r_N) \\ F_b(r_N) \end{pmatrix} \tag{4.8}$$

where F_a and F_b are defined in eq. (4.7). A trial solution $\vec{X}^{(0)}$ is given, and the system $\vec{F}(\vec{X}^{(0)})$ is solved using the standard Newton-Raphson method to produces corrections to the trial solution. These are applied to $\vec{X}^{(0)}$ to get an improved solution $\vec{X}^{(1)}$. The Newton–Raphson iteraction procedure reads

$$X^{(k+1)} = X^{(k)} - \left[DF(\vec{X}^{(k)}) \right]^{-1} \cdot \vec{F}(\vec{X}^{(k)}) \tag{4.9}$$

where $DF(\vec{X})$ is the $2N \times 2N$ matrix of space–time derivatives, until the fractional change between the last two iterations drops below an assigned threshold. Boundary conditions are imposed at each step. Relative accuracies of order $\approx 10^{-10}$ can be reached in 4–5 iterations for a good choice of the trial solution.

This method—known in astrophysics as the *Henyey scheme* [HVB65]—is used instead of a simpler explicit one (like Runge–Kutta) for many reasons:

- the initial temperature and luminosity profiles are not known *a priori*, so the problem cannot be treated as an initial values one;
- explicit methods are deemed to obey the Courant condition to be stable, i.e., the time step must be small enough for them to converge. This problem involves very different time scales: microscopic processes require scales of less than one second, while the evolution lasts $\sim 10^6$ y. This means that the timestep required for convergence must be so short to become computationally inefficient. On the other hand, implicit schemes are unconditionally stable for parabolic problems;
- it is fast: the computation of a cooling curve requires roughly one minute on a standard personal computer, while computations with explicit methods to obtain fig. 4.2 were a factor $\gtrsim 10$ slower and brute–force implicit methods did not converge at all in a reasonable time (≈hours).

Since variables acquire values in a range several orders of magnitude wide, logarithmic variables were used for integration.

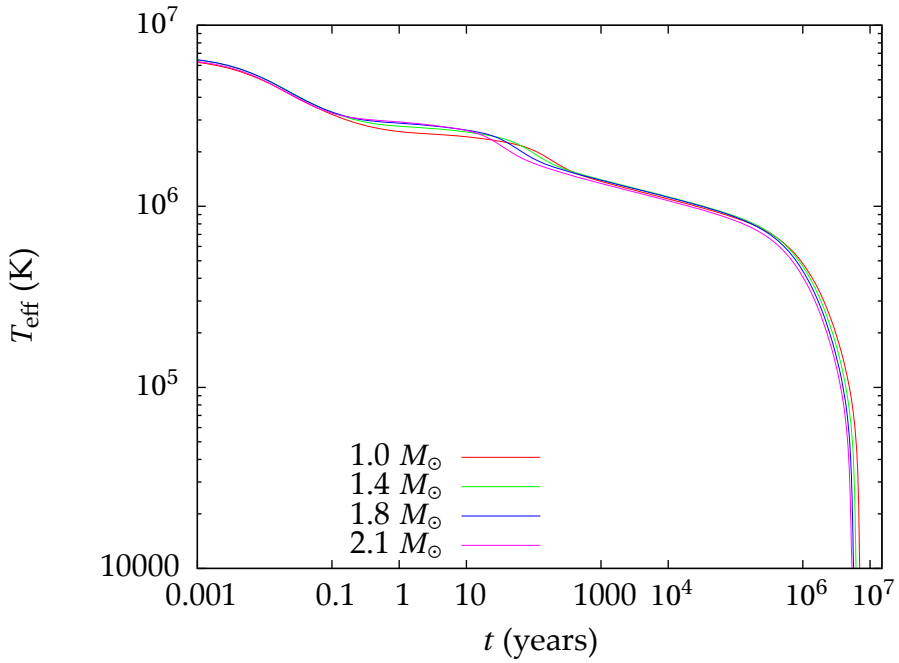

Figure 4.3: Cooling curves for non–SF slow cooling with APR EoS.

4.2.1 Slow cooling

Cooling curves for APR EoS (that will be used as a reference) are shown in fig. 5.4 for different total mass values. Direct Urca reactions are not allowed, hence this is an example of slow cooling. From this profile, different stages of cooling can be distinguished:

- for $t \lesssim 100\,\mathrm{y}$ a plateau is present. This is the phase dominated by the emission of plasma neutrinos from the crust;
- in $t \sim 100\,\mathrm{y}$ a steeper descent of temperature marks the isothermalization of the core. From this moment on, cooling is well described by power laws close to those predicted by eq. (4.3) and eq. (4.4);
- for $t \lesssim 10^5\,\mathrm{y}$ cooling is dominated by neutrino emission from the core;
- in the latest stages, cooling is given by blackbody–like photon emission.

Figure 4.4 shows a cooling curve compared to power–law curves obtained in simplified regimes. Besides the ones described in previous sections, it is shown a curve obtained considering an approximated form of the term describing heat

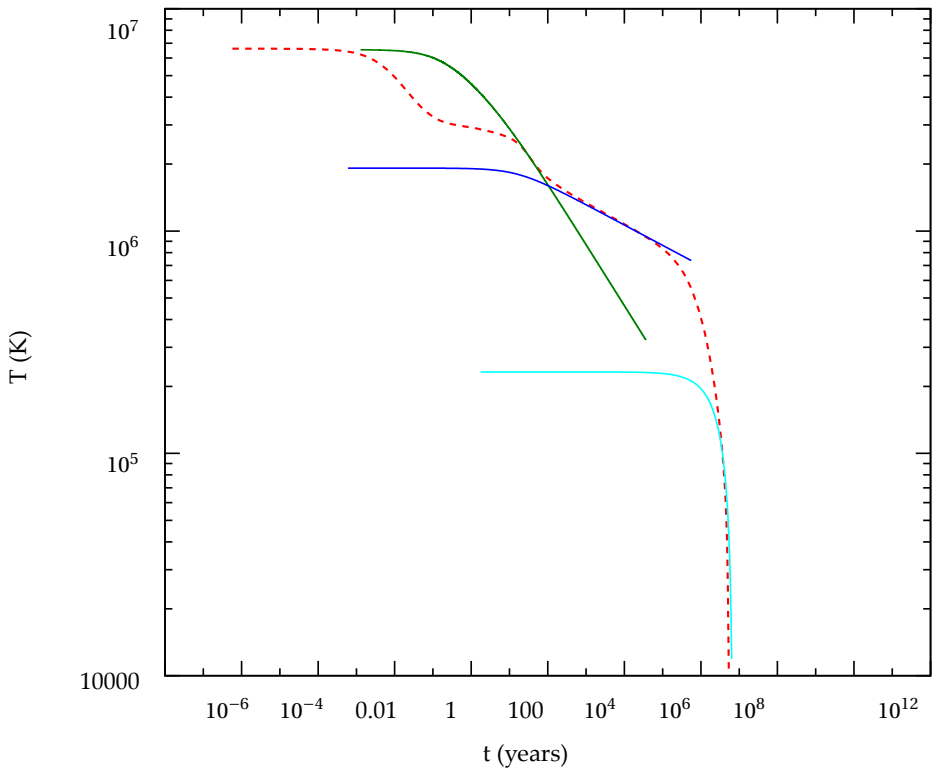

Figure 4.4: Example of a cooling curve (red dashed line) compared with power–laws for single stages: the blue curve refers to mUrca, the cyan curve to photon cooling, the green curve to the core conduction term (see text). Initial conditions for power–law curves were chosen arbitrarily to match the complete solution.

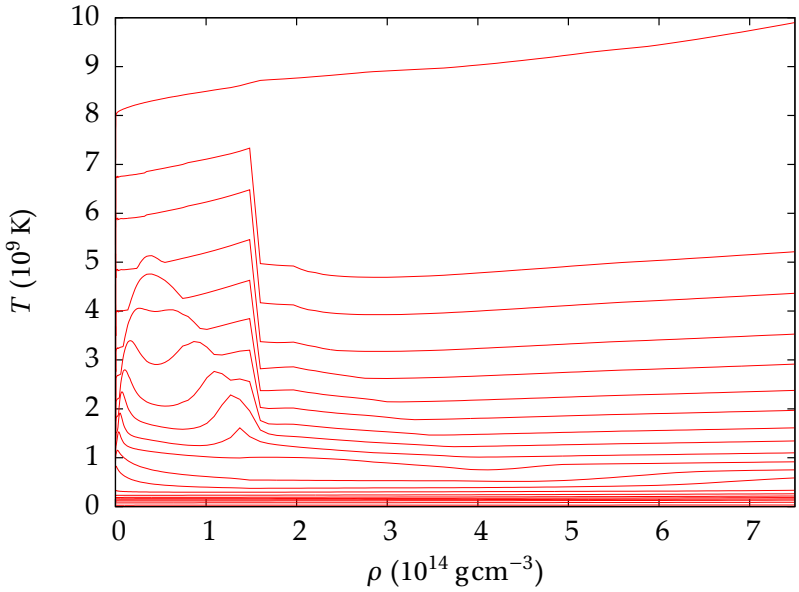

Figure 4.5: Internal temperature profile for a $1.0 M_\odot$ NS at different times (curves are separated by a logarithmic time step of $\Delta t/t = 3$). Note that the profile is shown as a function of density, so the most internal regions are on the right.

conduction in the core,

$$\int \mathrm{d}V \frac{\partial}{\partial r}\left(\frac{\mathscr{R}}{\sqrt{V}}\kappa\frac{\partial}{\partial r}(\sqrt{V}\,T)\right) \approx \mathscr{R} R \kappa T \tag{4.10}$$

where the radial dependence of κ was neglected. Even though this assumption is very rough, this curves matches the slope in region of core isothermalization, around $t \simeq 100\,\mathrm{y}$. The other power law slopes are also well matched.

The internal temperature profile is shown in fig. 4.5. The general tendency is that to go towards an isothermal object, with some difference from the crust to the core. In fact, isothermalization is much faster in the core than in the crust, where specific heat and conductivity are smaller*. In any case, by the beginning of the photon cooling stage the object can be considered isothermal as a whole.

*The study of transport phenomena in the crust is an active research field by itself, going beyond the purposes of this work. For the crustal values of c_v and κ a standard Fortran 90 routine has been used, as found in `http://www.ioffe.ru/astro/conduct/` [PPP15].

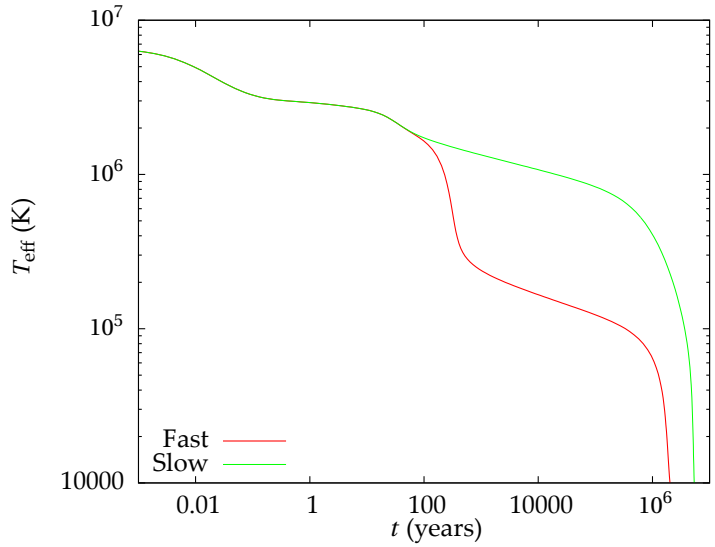

Figure 4.6: Cooling curves for the same $1M_\odot$ star with the same initial temperature in fast or slow cooling scenarios.

4.2.2 Fast Cooling

Direct Urca processes were not considered so far, since the APR EoS used as an example does not allow them. Nevertheless, to compare the different scenarios without changing the EoS, the kinematic threshold was artificially overcome in the inner core in the APR EoS. In fig. 4.6 the cooling curve for the same $1M_\odot$ star in the two scenarios is shown. Even if a certain EoS allows dUrca processes, they will not be present in all the NSs built from it, but only in the most massive ones. This minimum mass value for dUrca processes is a feature of the EoS itself. At the present time, there are no observations from which an experimental value of this threshold can be inferred, and some information about it would be of extreme importance in constraining the EoS. This effect is shown in fig. 4.7, where the cooling curves of stars of different mass are shown. Once the dUrca threshold is passed, cooling curves have a different behaviour: after the first descent due to core isothermalization, they have another steep descent given by direct Urca. In this phase, they cool down almost one order of magnitude more than what slow–cooling stars do in the same time. Then, the curves become almost parallel again, but fast cooling curves are separated from the rest.

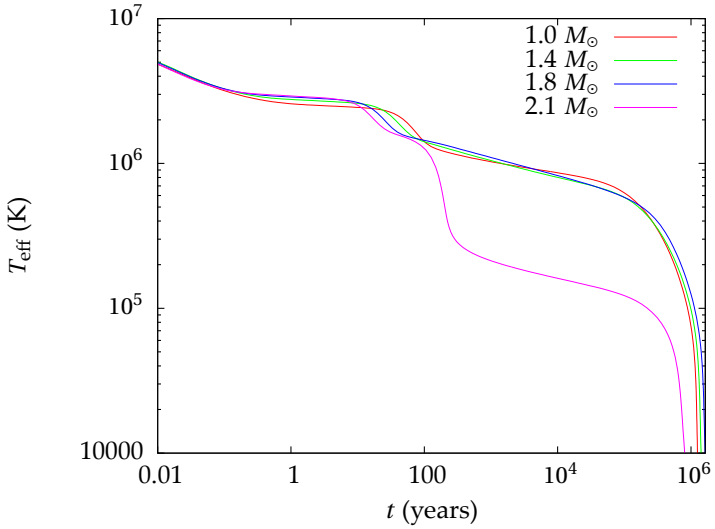

Figure 4.7: Cooling curves for different masses with the same EoS. The most massive star experiences fast cooling.

5 | Cooling of SF NSs

In chapter 2 the presence of a superfluid nucleon phase in the NS was considered, and convenient reduction factors were introduced to describe its effects. In this chapter the implications for NS cooling will be addressed.

5.1 Cooling curves

Superfluidity manifest itself in the modification of transport properties of matter and of reaction rates; as an example, in fig. 5.1 the values of the SF factors for mUrca reactions and specific heat for ${}^1S_0$ superfluidity are shown as functions of the reduced temperature $\tau = T/T_c$.

Since superfluidity reduces the emissivities, one may intuitively expect a reduction of cooling. However, the alteration of transport phenomena described by $\mathfrak{R}_{cv}$ and $\mathfrak{R}_\kappa$ is a stronger effect, so that superfluidity *enhances* cooling. To study this fact isolating the various effects, we can return to the isothermal approximation by solving eq. (4.2) with the values of the integrals from eq. (4.5) calculated considering SF reduction factors. The results are shown in fig. 5.2:

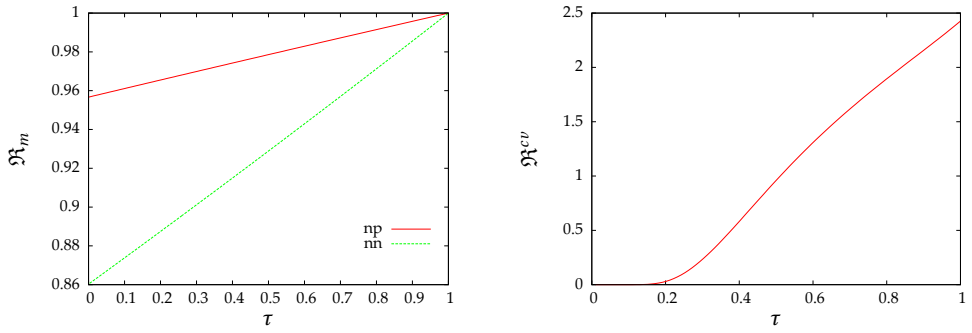

(a) *Modified Urca reactions reduction factor.* (b) *Specific heat SF factor.*

Figure 5.1: Some example of ${}^1S_0$ SF factors.

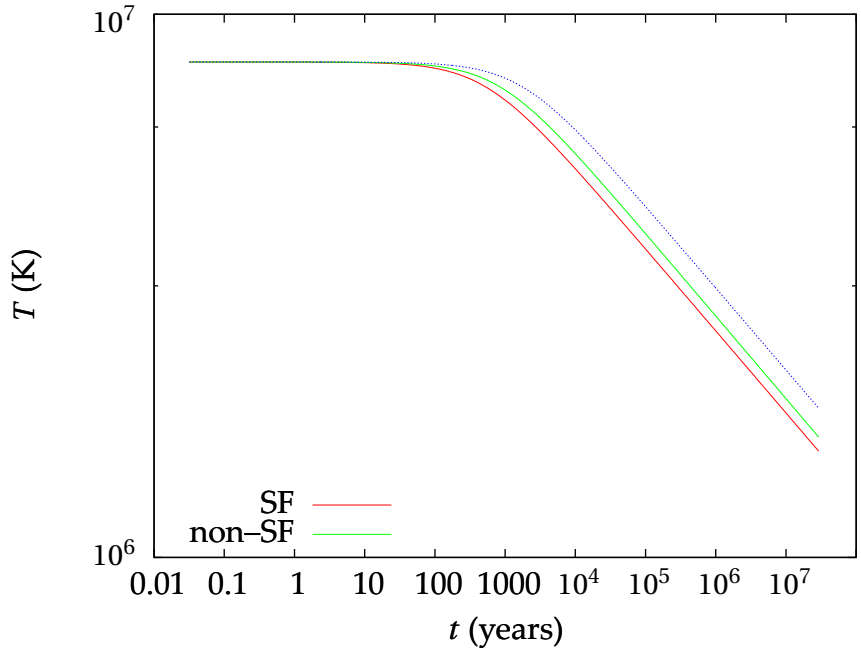

Figure 5.2: Isothermal–core slow cooling with or without SF effects. The dashed line shows the cooling profile obtained without taking into account the modification of the specific heat but SF neutrino reaction reduction factors only.

if the SF reduction of neutrino emission is considered alone, a slower cooling profile is produced, whereas taking into account also the reduction of c_ν (κ is not considered in isothermal approximation) the opposite effect is obtained: cooling is enhanced. No SF reactions like in eq. (2.39) are taken into account in this simplified treatment.

Conversely, fig. 5.4 shows the effect of superfluidity on a cooling curve built from the complete equations. The curves obtained with or without SF effects split during the core isothermalization phase, controlled by κ, and cooling is enhanced in the following phases as well. The slope of neutrino and photon cooling phases are not substantially altered, since the power dependences of reaction rates are not altered but for the $\sim T^7$ term due to the reactions of eq. (2.39), which are not the dominant effect. Therefore, the thermal evolution proceeds in a qualitatively similar fashion, but with a faster pace.

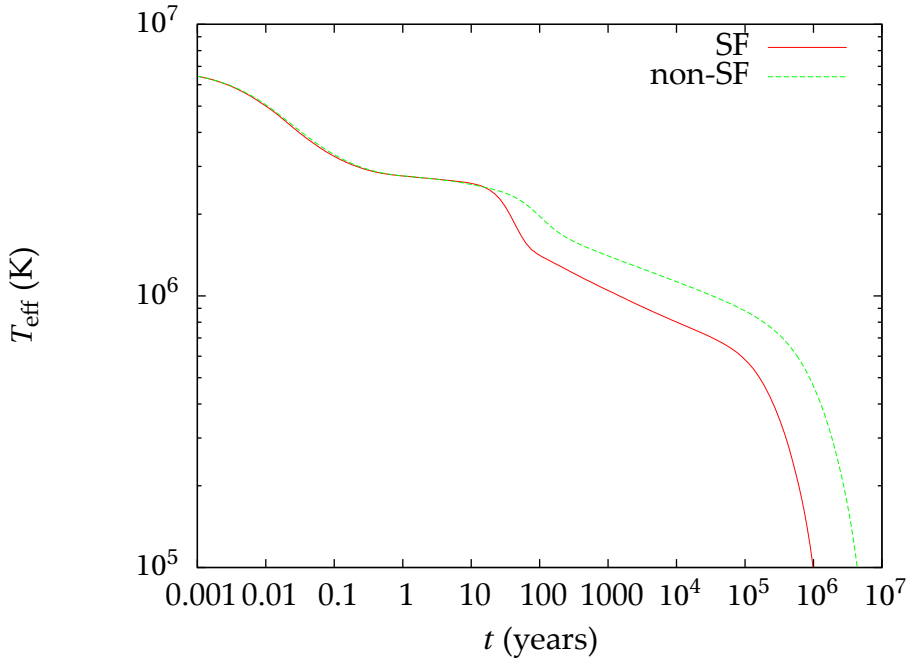

Figure 5.3: Cooling curve for the same $1.4 M_\odot$ star (with APR EoS) with or without SF effects. Superfluidity enhances cooling.

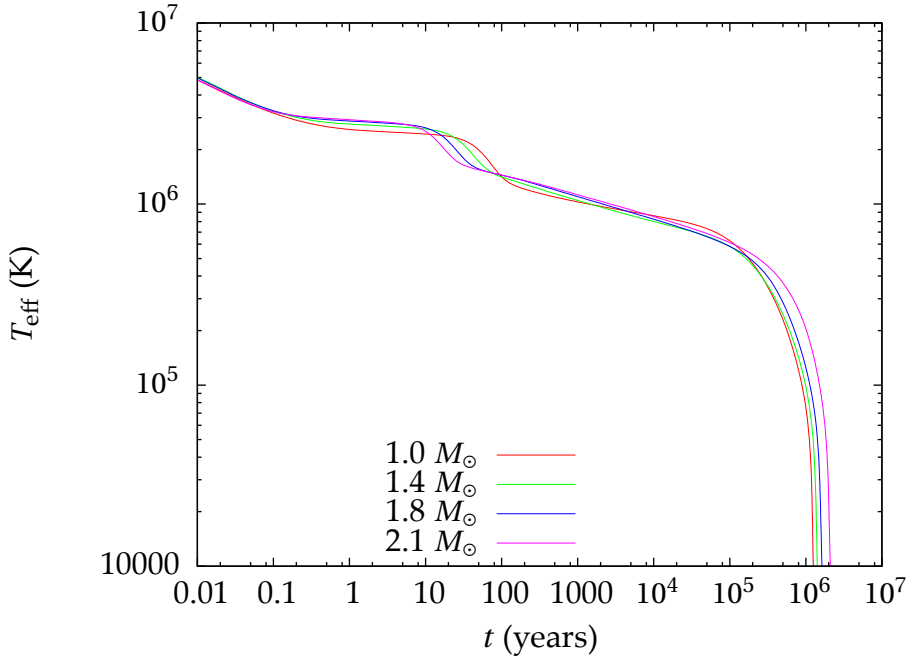

Figure 5.4: Cooling curves for SF slow cooling with APR EoS.

5.2 Comparison with data

Observations of NSs are very difficult to perform, since they are very dim sources often emitting in bands that are not accessible to ground–based instruments. In fact, some NSs emit optical or infrared radiation but for our purposes the most interesting information is in the thermal component, which has the form of a black–body, that is emitted in the X–ray band. Moreover, to study the thermal evolution of the object the thermal component of the emission must be isolated from other contributions coming from the surrounding magnetosphere, mainly busting events and synchrotron radiation, which have the form of a power law. During violent events a thermal component may appear in the spectrum due to the heating of small regions of the star, and one must pay attention to separate it from the persistent thermal component that must be used to follow the thermal evolution.

Table 5.1 shows data of the objects for which a thermal emission component has been detected and studied using data from the XMM and CHANDRA satellites. They are plotted in fig. 5.5 together with the cooling curves obtained for SF cooling. The magneto–rotational characteristic age τ (see eq. (1.2)) has been assumed to coincide with the age of the stars. Cooling curves, of course, depend on the initial temperature of the object which cannot be derived directly from observations. Therefore, the cooling curves are plotted with the same initial value of surface temperature $T_{s,0} = 7.5 \times 10^6\,\mathrm{K}$ that is representative of the range of values compatible with data. Hence, the plot must be taken with some care, since a small temperature offset should in principle be put for each star.

Nevertheless, the comparison of the cooling curves with data highlights some key features. First, different NS populations behave differently: while Pulsars and XDINSs lay in a range compatible with the predicted cooling curves, Magnetars and CCOs (*Central Compact Objects*, i.e., NSs found at the center of a SN remnant) are much hotter than what predicted. This is due to the presence of a heating mechanism: in magnetars it is the ohmic dissipation of the magnetic field, while in CCO it is due to episodes of fall–back accretion of the surrounding material onto the NS. High–magnetic field pulsars also show temperatures higher than expected, even if their number is not large enough to infer general properties. It should also be mentioned that the magneto–rotational characteristic age is not a reliable estimator of the age for magnetars, since it is calculated in the assumption of constant magnetic field, while in magnetars a substantial decay of the magnetic field occours [TZW15].

Moreover, the figure shows the fast cooling curve (black line) of fig. 4.7 alongside the slow cooling ones. Even though the quantity and quality of data cannot give a definite conclusion about it, the fast cooling scenario does not seem

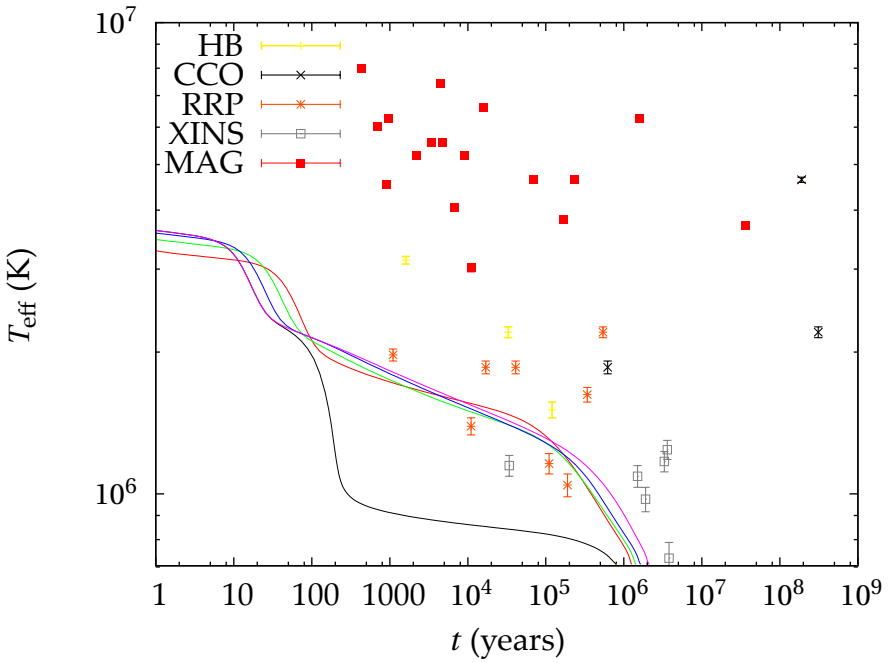

Figure 5.5: Cooling curve for SF slow cooling with APR EoS and an initial temperature of 7.5×10^6 K compared with data in table 5.1.

compatible with observations. This excludes the presence of dUrca reactions of all kinds, the ordinary neutrino ones as well as the ones involving exotica. This puts a double constraint on the EoS. First, the minimum threshold mass value for which dUrca neutrino precesses are possible should not be present or, at least, it should be higher than the mass of the observed objects, even if an observational limit cannot be put since mass measurements of an isolated NS cannot be made reliably but in very few cases. Second, the possibility of the appearance of an exotic phase in the inner core is greatly disfavoured.

Then, according to the more recent data the *minimal cooling* model, i.e., cooling due to mUrca and bremsstrahlung reactions with a superfluid phase is consistent with the observations of isolated pulsars, while other objects require a different approach, which however does not involve dUrca processes.

Object	Class	P (s)	$\dot{P}$ (s/s)	B_p (G)	τ (y)	$k_b T$ (eV)
CXOU J185238.6+004020	CCO	0.105	8.7×10^{-18}	6.1×10^{10}	1.90×10^{8}	440
1E 1207.4-5209		0.424	2.2×10^{-17}	2.0×10^{11}	3.10×10^{8}	190
RX J0822-4300		0.112	9.3×10^{-18}	6.5×10^{10}	1.90×10^{8}	400
PSR J0538+2817	RRP	0.143	3.7×10^{-15}	1.5×10^{12}	6.20×10^{5}	160
PSR B1055-52		0.197	5.8×10^{-15}	2.2×10^{12}	5.40×10^{5}	190
PSR J0633+1746		0.237	1.1×10^{-14}	3.3×10^{12}	3.40×10^{5}	140
PSR B1706-44		0.102	9.3×10^{-14}	6.2×10^{12}	1.70×10^{4}	160
PSR B0833-45		0.089	1.2×10^{-13}	6.8×10^{12}	1.10×10^{4}	120
PSR B0656+14		0.385	5.5×10^{-14}	9.3×10^{12}	1.10×10^{5}	100
PSR B2334+61		0.495	1.9×10^{-13}	2.0×10^{13}	4.10×10^{4}	160
PSR J1740+1000		0.154	2.1×10^{-12}	3.7×10^{13}	1.10×10^{3}	170
PSR J0726-2612		3.440	2.9×10^{-13}	6.4×10^{13}	1.90×10^{5}	90
PSR J1119-6127	HB	0.408	4.0×10^{-12}	8.2×10^{13}	1.60×10^{3}	270
PSR J1819-1458		4.263	5.7×10^{-13}	1.0×10^{14}	1.20×10^{5}	130
PSR J1718-3718		3.378	1.6×10^{-12}	1.5×10^{14}	3.30×10^{4}	190
RX J0420.0-5022	XDINS	3.450	2.8×10^{-14}	2.0×10^{13}	2.00×10^{6}	50
RX J1856.5-3754		7.055	3.0×10^{-14}	2.9×10^{13}	3.80×10^{6}	63
RX J2143.0+0654		9.428	4.1×10^{-14}	4.0×10^{13}	3.60×10^{6}	107
RX J0720.4-3125		8.391	6.9×10^{-14}	4.9×10^{13}	1.90×10^{6}	84
RX J0806.4-4123		11.370	5.5×10^{-14}	5.1×10^{13}	3.30×10^{6}	101
RX J1308.6+2127		10.310	1.1×10^{-13}	6.8×10^{13}	1.50×10^{6}	94
RX J1605.3+3249		3.390	1.6×10^{-12}	1.5×10^{14}	3.40×10^{4}	99
1E 2259+586	MAG	6.979	4.8×10^{-13}	1.2×10^{14}	2.30×10^{5}	400
4U 0142+614		8.689	2.0×10^{-12}	2.7×10^{14}	6.90×10^{4}	400
CXO J164710.2-455216		10.611	9.7×10^{-13}	2.1×10^{14}	1.70×10^{5}	330
XTE J1810-197		5.540	7.8×10^{-12}	4.2×10^{14}	1.10×10^{4}	260
1E 1547.0-5408		2.072	4.7×10^{-11}	6.3×10^{14}	7.00×10^{2}	520
1E 1048.1-5937		6.458	2.2×10^{-11}	7.7×10^{14}	4.50×10^{3}	640
CXOU J010043.1-721		8.020	1.9×10^{-11}	7.9×10^{14}	6.80×10^{3}	350
1RXS J170849.0-400910		11.003	1.9×10^{-11}	9.3×10^{14}	9.10×10^{3}	450
CXOU J171405.7-381031		3.825	6.4×10^{-11}	1.0×10^{15}	9.50×10^{2}	540
1E 1841-045		11.782	3.9×10^{-11}	1.4×10^{15}	4.80×10^{3}	480
SGR 0501+4516		5.762	5.8×10^{-12}	3.7×10^{14}	1.60×10^{4}	570
SGR 1627-41		2.595	1.9×10^{-11}	4.5×10^{14}	2.20×10^{3}	450
SGR 0526-66		8.054	3.8×10^{-11}	1.1×10^{15}	3.40×10^{3}	480
SGR 1900+14		5.200	9.2×10^{-11}	1.4×10^{15}	9.00×10^{2}	390
SGR 1806-20		7.602	2.7×10^{-10}	2.9×10^{15}	4.40×10^{2}	690
SGR 0418+5729		9.078	4.0×10^{-15}	1.2×10^{13}	3.60×10^{7}	320
Swift J1822.3-1606		8.438	8.3×10^{-14}	5.4×10^{13}	1.60×10^{6}	540

Table 5.1: Observational data for cooling NSs from `http://www.neutronstarcooling.info`. B_p is the value of the magnetic field at the magnetic pole. Classes are labeled by: CCO for *central compact objects*, RRP for *rotating radio pulsars*, HB for *high magnetic fild pulsars*, XDINS for *X–ray isolated NSs* and MAG for *magnetars*.

6 | Conclusions and Future Perspectives

This thesis focused on the study of the thermal evolution of isolated neutron stars (NSs), assessing and comparing the role of different cooling processes. NSs are born very hot in the aftermath of the core-collapse and then cool down. In the early phases of their history, cooling occurs mainly via neutrino losses through two possible channels, the so-called fast (direct Urca) and slow (modified Urca) processes. Discriminating between the two scenarios is of key importance since it directly impacts on the composition of the inner regions of the NS, and hence on the equation of state (EoS) of ultra-dense matter, a still major open issue in compact object astrophysics.

The possibility that the star core contains a superfluid phase appears likely, although details depend somehow on the choice of the superfluid gap. The presence of a superfluid with creation of Cooper pairs strongly influences neutrino cooling, resulting in the *minimal cooling* scenario, that includes modified Urca processes and neutrino bremsstrahlung [Pag+04]. This minimal cooling scenario turns out to be more efficient than the slow cooling, without resorting to the presence of exotic phases necessary for the onset of fast cooling.

We investigated NS thermal history both in the case of fast and slow cooling, either including or not superfluid effects, accounting also for the early crustal and the late photon cooling stages. This was obtained by solving numerically the general relativistic heat transport equation, using a relaxation technique (Henyey scheme), adapted to parabolic PDEs. The assumption of low magnetization allowed us to treat the problem in spherical symmetry, i.e. in one dimension.

We compared the different cooling curves with the set of existing data for isolated NSs from which thermal emission has been detected, and hence a measure of the surface temperature and of the age was possible. The main conclusion is that the minimal cooling scenario is consistent with observations, confirming the early findings. No observational evidence for the occurrence of fast cooling was found, disfavouring the presence of exotic phases in the core.

The cooling models investigated in this thesis fail, however, to explain the observations of some classes of isolated NSs, in particular the magnetars. These objects are believed to host an ultra-strong magnetic field ($B \gtrsim 10^{13}$ G), the evolu-

tion of which plays an important role in providing an additional source of heat which was not considered here. Moreover, the presence of a strong, decaying magnetic field requires to solve the coupled thermal and magnetic evolution. This must be tackled using a much more sophisticated multi-dimensional approach, since spherical symmetry can not be assumed anymore, and was outside the scope of the present work. Some 2D models have already been presented in the literature (see e.g. [APM08], [Vig13]), whereas 3D models are currently under development [GWH16].

The NS interior can also be used as an ideal laboratory where to test the predictions of the Standard Model of particle physics and its extreme. Nonetheless, to push forward comparison with observations more reliable data are necessary to tightly constrain cooling models and remove degeneracies in the parameter space. This constitutes an observational and technical challenge for upcoming space missions, like the ESA X-ray satellite Athena.

NSs are also one of the main targets for the uprising Multimessenger Astrophysics: the direct detection of neutrinos emitted by a cooling NS has never been performed as yet. Information on the physical condition of the NS interior have also been provided by the simultaneous gravitational-wave and electromagnetic observation in the NS merging event GW-GRB170817. More are expected to follow soon, as the upgrading of the LIGO/VIRGO detectors will be completed.

These studies place themselves within the framework of the Grand Unification of NSs [KRH10]. Such a theory should be able to explain the variety of NS populations and phenomenology. In particular, the most relevant open issue is whether the different NS types we can observe today are essentially different one from each other—due, for example, to the different conditions of the progenitor star—or an evolutionary link between at least some of the classes can be found, so that what we see today reflects the various phases which a "unified NS" can pass through its history. A complete theory of NS evolution should also account for the vast phenomenology of Gamma and X–ray bursting events coming from these objects. Modeling the internal structure of a NS is a key point to follow its magneto–thermal evolution, finding possible links between different population towards the unified model.

Bibliography

[APM08] Deborah N. Aguilera, Jose A. Pons, and Juan A. Miralles. "2D Cooling of Magnetized Neutron Stars". In: *Astron. Astrophys.* 486 (2008), pp. 255–271.

[APR98] A. Akmal, V. R. Pandharipande, and D. G. Ravenhall. "Equation of state of nucleon matter and neutron star structure". In: *Phys. Rev. C* 58 (3 Sept. 1998), pp. 1804–1828.

[ASA05] B. K. Agrawal, S. Shlomo, and V. Kim Au. "Determination of the parameters of a Skyrme type effective interaction using the simulated annealing approach". In: *Phys. Rev. C* 72 (1 July 2005), p. 014310.

[BCS57] J. Bardeen, L. N. Cooper, and J. R. Schrieffer. "Microscopic Theory of Superconductivity". In: *Physical Review* 106 (Apr. 1957), pp. 162–164.

[BHY01] D. A. Baiko, P. Haensel, and D. G. Yakovlev. "Thermal conductivity of neutrons in neutron star cores". In: *A&A* 374 (July 2001), pp. 151–163.

[BS93] E. Braaten and D. Segel. "Neutrino Energy loss from Plasma Processes at all Temperatures". In: *Phys. Rew, D* 48 (1993), pp. 1478–1491.

[CompOSE] URL: `https://compose.obspm.fr/home/`.

[DP+10] P. B. Demorest, T. Pennucci, et al. "A two-solar-mass neutron star measured using Shapiro delay". In: *Nature* 467 (2010), p. 1081.

[DSW83] R. C. Duncan, S. L. Shapiro, and I. Wasserman. "Equilibrium composition and neutrino emissivity of interacting quark matter in neutron stars". In: *ApJ* 267 (Apr. 1983), pp. 358–370.

[FI79] E. Flowers and N. Itoh. "Transport properties of dense matter. II". In: *ApJ* 230 (June 1979), pp. 847–858.

[FM79] B. L. Friman and O. V. Maxwell. "Neutrino Emissivities of Neutron Stars". In: *ApJ* 232 (1979), pp. 541–557.

[GPE83] E. H. Gudmundsson, C. J. Pethick, and R. I. Epstein. "Structure of neutron star envelopes". In: *ApJ* 272 (Sept. 1983), pp. 286–300.

[GR15] F. Gulminelli and Ad. R. Raduta. "Unified treatment of subsaturation stellar matter at zero and finite temperature". In: *Phys. Rev.* C92.5 (2015), p. 055803.

[GS41] G. Gamow and M. Schoenberg. "Neutrino Theory of Stellar Collapse". In: *Phys. Rev.* 59 (7 Apr. 1941), pp. 539–547.

[Gus+04] M. E. Gusakov et al. "Enhanced cooling of neutron stars via Cooper pair neutrino emission". In: *A&A* 423 (2004), pp. 1063–1071.

[GWH16] K. N. Gourgouliatos, T. S. Wood, and R. Hollerbach. "Magnetic field evolution in magnetar crusts through three-dimensional simulations". In: *Proceedings of the National Academy of Science* 113 (Apr. 2016), pp. 3944–3949.

[GY95] O.Y. Gnedin and D.G. Yakovlev. "Thermal conductivity of electrons and muons in neutron star cores". In: *Nuclear Physics A* 582.3 (1995), pp. 697–716.

[HN12] Glampedakis K. Ho W. C. G. and Andersson N. "Magnetars: super(ficially) hot and super(fluid) cool". In: *MNRAS* 422 (2012), p. 2632.

[HPY07] P. Haensel, A. Y. Potekhin, and D. G. Yakovlev. *Neutron Stars 1*. 2007.

[HVB65] L. Henyey, M. S. Vardya, and P. Bodenheimer. "Studies in Stellar Evolution. III. The Calculation of Model Envelopes." In: *ApJ* 142 (Oct. 1965), p. 841.

[Iwa82] Naoki Iwamoto. "Neutrino emissivities and mean free paths of degenerate quark matter". In: *Annals of Physics* 141.1 (1982), pp. 1–49.

[Ker63] Roy P. Kerr. "Gravitational Field of a Spinning Mass as an Example of Algebraically Special Metrics". In: *Phys. Rev. Letters* 11 (1963), pp. 237–238.

[KHY01] Kaminker, A. D., Haensel, P., and Yakovlev, D. G. "Nucleon superfluidity vs. observations of cooling neutron stars". In: *A&A* 373.2 (2001), pp. L17–L20.

[KRH10] V. M. Kaspi, M. S. E. Roberts, and A. K. Harding. "Isolated neutron stars". In: *Compact Stellar X-ray Sources*. Ed. by W. Lewin and M. van der Klis. Nov. 2010, p. 279.

[Lan37] Lev D. Landau. "Origin of Stellar Energy". In: *Doklady Akad. Nauk SSSR* 17 (1937), p. 301.

[LLP77] Lev D. Landau, E. M. Lifshitz, and L. P. Pitaevskij. *Course of Theoretical Physics vol. 9: Statistical Physics II*. 1977.

[LY94] K. P. Levenfish and D. G. Yakovlev. "Specific heat of neutron star cores with superfluid nucleons". In: *Astronomy Reports* 38 (Mar. 1994), pp. 247–251.

[NT88] L. Nobili and R. Turolla. "Henyey method revisited: an application to problems involving critical points". In: *ApJ* 333 (1988), pp. 248–255.

[OV39] J.R. Oppenheimer and G.M. Volkoff. "On Massive neutron cores". In: *Phys. Rev.* 55 (1939), pp. 374–381.

[Pag+04] Dany Page et al. "Minimal cooling of neutron stars: A New paradigm". In: *Astrophys. J. Suppl.* 155 (2004), pp. 623–650.

[Pag98] D. Page. "Thermal Evolution of Isolated Neutron Stars". In: *Neutron Stars and Pulsars: Thirty Years after the Discovery*. Ed. by N. Shibazaki. 1998, p. 183.

[PPP15] A. Y. Potekhin, J. A. Pons, and D. Page. "Neutron Stars—Cooling and Transport". In: *Space Sience Reviews* 191 (Oct. 2015), pp. 239–291.

[RF95] P.-G. Reinhard and H. Flocard. "Nuclear effective forces and isotope shifts". In: *Nuclear Physics A* 584.3 (1995), pp. 467–488. ISSN: 0375-9474.

[RPW83] D. G. Ravenhall, C. J. Pethick, and J. R. Wilson. "Structure of Matter below Nuclear Saturation Density". In: *Phys. Rev. Lett.* 50 (26 June 1983), pp. 2066–2069.

[Sca69] J. D. Scargle. "The Center of Activity in the Crab Nebula". In: *AP Letters* 3 (1969), p. 73.

[Sch16] Karl Schwarzschild. "On the gravitational field of a mass point according to Einstein's theory". In: *Sitzungsber.Preuss.Akad.Wiss.Berlin (Math.Phys.)* 1916 (1916), pp. 189–196.

[She+98] H. Shen et al. "Relativistic equation of state of nuclear matter for supernova explosion". In: *Prog. Theor. Phys.* 100 (1998), p. 1013.

[ST83] S. L. Shapiro and S. A. Teukolsky. *Black Holes, White Dwarfs and Neutron Stars. The Physics of Compact Objects*. 1983.

[Tho77] Kip S. Thorne. “The relativistic equations of stellar structure and evolution”. In: *ApJ* 212 (1977), pp. 825–831.

[Tsu64] S. Tsuruta. “Neutron Star Models”. PhD thesis. New York, N.Y.: Columbia University, 1964.

[TZW15] R. Turolla, S. Zane, and A. L. Watts. “Magnetars: the physics behind observations. A review”. In: *Reports on Progress in Physics* 78.11 (2015), p. 116901.

[Vig13] D. Viganò. “Magnetic Fields and Neutron Stars”. PhD thesis. Universidad de Alicante, 2013.

[Wei64] S. Weinberg. “A model of leptons”. In: *Phys. Rev.* (1964).

[Wit84] Edward Witten. “Cosmic separation of phases”. In: *Phys. Rev. D* 30 (2 July 1984), pp. 272–285.

[YGH01] D. G. Yakovlev, O. Y. Gnedin, and P. Haensel. “Neutrino Emission from Neutron Stars”. In: *Physics Reports* 354 (2001), pp. 1–155.

[Zwi33] Fritz Zwicky. “Supernovae and Cosmic Rays”. In: *Proc. of Am. Phys. Soc.* 45 (1933).